CZECH TECHNICAL UNIVERSITY IN PRAGUE

Faculty of Civil Engineering

Department of Mechanics

Micromechanical study of spruce wood

Master's Thesis

Study Programme:	Civil Engineering (Czech)
Branch of Study:	Building structures
Supervisor:	Prof. Ing. Michal Šejnoha, Ph.D., DSc.

Bc. Lucie Kucíková

Prague 2018

ČESKÉ VYSOKÉ UČENÍ TECHNICKÉ V PRAZE
Fakulta stavební
Thákurova 7, 166 29 Praha 6

ZADÁNÍ DIPLOMOVÉ PRÁCE

I. OSOBNÍ A STUDIJNÍ ÚDAJE

Příjmení: Kucíková Jméno: Lucie Osobní číslo: 412638

Zadávající katedra: K132 - Katedra mechaniky

Studijní program: (N3607) Stavební inženýrství

Studijní obor: (3608T008) Konstrukce pozemních staveb

II. ÚDAJE K DIPLOMOVÉ PRÁCI

Název diplomové práce: Mikromechanická studie smrkového dřeva

Název diplomové práce anglicky: Micromechanical study of spruce wood

Pokyny pro vypracování:
- v anglickém jazyce
- Stanoveni efektivních elastických vlastností, stanovení MFA na základě výsledků z nanoindentace
- Stanovení efektivních transportních parametrů
- Studie vlivu mikrostruktury na mechanické a transportní vlastnosti
- Porovnání výpočtu s experimentem

Seznam doporučené literatury:
M. Šejnoha and J. Zeman, Micromechanics in Practice, WIT Press, 2013

Jméno vedoucího diplomové práce: Prof. Ing. Michal Šejnoha, Ph.D., DSc.

Datum zadání diplomové práce: 19.9.2017 Termín odevzdání diplomové práce: 7.1.2018
Údaj uveďte v souladu s datem v časovém plánu příslušného ak. roku

Podpis vedoucího práce Podpis vedoucího katedry

III. PŘEVZETÍ ZADÁNÍ

Beru na vědomí, že jsem povinen vypracovat diplomovou práci samostatně, bez cizí pomoci, s výjimkou poskytnutých konzultací. Seznam použité literatury, jiných pramenů a jmen konzultantů je nutné uvést v diplomové práci a při citování postupovat v souladu s metodickou příručkou ČVUT „Jak psát vysokoškolské závěrečné práce" a metodickým pokynem ČVUT „O dodržování etických principů při přípravě vysokoškolských závěrečných prací".

19.9.2017
Datum převzetí zadání Podpis studenta(ky)

SPECIFIKACE ZADÁNÍ

Jméno diplomanta: Lucie Kucíková

Název diplomové práce: Micromechanical study of spruce wood

Základní část: ..... podíl: 100 %

Formulace úkolů:
1. Popis mikrostruktury smrkového dřeva, návrh vhodného výpočetního modelu a identifikace rozhodujících parametrů pro popis mikrostruktury dřeva.
2. Stanovení efektivních elastických, transportních a hygroskopických vlastností smrkového dřeva s využitím klasických nástrojů mikromechaniky.
3. Porovnání výsledků teoretické predikce s experimentálním měřením.
4. Posouzení vhodnosti navrženého modelu.

Podpis vedoucího DP: ..... Datum: 19.9.2017

Případné další části diplomové práce (části a jejich podíl určí vedoucí DP):

2. Část: ..... podíl: ..... %

Konzultant (jméno, katedra): .....

Formulace úkolů:

Podpis konzultanta: ..... Datum:.....

3. Část: ..... podíl: ..... %

Konzultant (jméno, katedra: .....

Formulace úkolů:

Podpis konzultanta: ..... Datum: .....

4. Část: ..... podíl: ..... %

Konzultant (jméno, katedra): .....

Formulace úkolů:

Podpis konzultanta: ..... Datum: .....

Poznámka:
Zadání včetně vyplněných specifikací je nedílnou součástí diplomové práce a musí být přiloženo k odevzdané práci.
(Vyplněné specifikace není nutné odevzdat na studijní oddělení spolu s 1.stranou zadání již ve 2.týdnu semestru)

Declaration of authorship

Hereby I declare that I have completed Master's thesis called "*Micromechanical study of spruce wood*" by myself and that I stated all information sources in accordance with the Methodological guideline of the Czech Technical University in Prague.

In Prague, January 8th, 2018

Bc. Lucie Kucíková

Acknowledgements

Firstly, I would like to gratefully acknowledge Prof. Ing. Michal Šejnoha, Ph.D., DSc. for the supervising of the Master's thesis and a big help with understanding of the issue. Next, I would like to thank doc. Ing. Jan Vorel, Ph.D. for a great help with computations. And last but not least, I would like to thank Ing. Vladimír Hrbek for the help with sample preparation and nanoindentation measurements, Ing. Pavel Padevět, Ph.D. for the tensile tests and Prof. Ing. Zbyšek Pavlík, Ph.D. for the measurement of moisture diffusion coefficients. The financial support provided by the GACR grant No. 15-10354S and by the Czech Technical University in Prague within SGS project with the application registered under the No. SGS17/168/OHK1/3T/11 is gratefully acknowledged.

Abstract

Title: Micromechanical study of spruce wood

The wood is a natural material widely used for building constructions. Although it has been used for centuries, its behaviour has not been fully examined, yet. Due to the development of laboratory technologies, it is possible to study the wood composition and its properties at the level of nanometres or lower. This thesis provides prediction of the wood properties using the micromechanical model based on real structural composition of spruce wood. The computation is performed by analytical homogenization methods, using classical Self-consistent scheme, Mori-Tanaka method and lamination theory. The model is supported by several experimental measurements. A comparison with numerical solution is also provided. Although, in some cases the calculated values were in good accordance with those measured, further development of the micromechanical model is still necessary.

Keywords: Spruce, Wood microstructure, Micromechanical homogenization, Mechanical properties, Moisture diffusion coefficient, Coefficient of thermal conductivity

Abstrakt

Název: Mikromechanická studie smrkového dřeva

Dřevo je přírodní materiál široce využívaný pro stavební konstrukce. Ačkoliv se používá již po staletí, jeho vlastnosti stále nejsou plně prozkoumány. Díky vývoji laboratorních technologií je možné studovat strukturu dřeva a jeho vlastnosti na úrovni nanometrů i nižší. Tato práce poskytuje predikci vlastností dřeva s využitím mikromechanického modelu, založeném na skutečné strukturní stavbě smrkového dřeva. Výpočet je proveden pomocí klasické Self-konzistentní metody, metody Mori-Tanaka a laminační teorie. Pro ověření modelu byla provedena řada laboratorních měření. V rámci práce je také provedeno porovnání s numerickým řešením. Ačkoliv v několika případech vykazovaly vypočtené hodnoty dobrou shodu s těmi naměřenými, je další vylepšení mikromechanického modelu nutné.

Klíčová slova: smrk, mikrostruktura dřeva, mikromechanická homogenizace, mechanické vlastnosti, součinitel difuze vodní páry, součinitel teplotní vodivosti

“We may use wood with intelligence only if we understand wood”

Frank Lloyd Wright (1928)

Content

1 Introduction

The wood is a natural building material used in construction for centuries. Its natural origin and renewability are of great advantage, particularly nowadays when environmental issues are at the forefront of the global interest. This fact caused an expansion of the logging industry. As an example, the timber production in the Czech Republic increased from 14.44x106 m^3 (2000) to 16.16x106 m^3 (2015) [1], which corresponds to an increment of 11.9 %, and it is reasonable to expect further growth. In 2015 the forests covered 36.8% of the total territory of the Czech Republic [1] and the major part comprises the Norway spruce (*Picea abies*) (50.6% of the forest area [1]). This thesis is mostly focused on spruce timber used for building construction.

Generally, the knowledge of the material properties is very important for a proper structural design. The wood is an anisotropic material, but it is possible to reduce the number of independent material constants on some scales. For example, the wood is usually considered as orthotropic on a macro scale. The determination of material constants could be very difficult, especially in the case of wood. It is well known that the wood properties rely on many aspects. Starting from a living tree, where growth conditions have an influence on the wood composition and subsequently on density; structural defects, e.g. knots, which are remains of dead or living branches; grain deviations or development of the reaction wood. Even the cut wood is dependent on ambient conditions, such as humidity and temperature. Humidity of the surroundings and consequently the moisture content has a significant impact on the wood properties. Thus, it is important to understand the moisture relations. One of the quantities governing the moisture movement is a moisture diffusivity. With increasing demands on energy savings and reduction of heat transmission through structures, it is necessary to observe another quantity, namely thermal conductivity. Proper design of the building is a very complex task including many variable parameters. It is almost impossible to implement all these variables into the computational model. The correct approach would be the introduction of the effective properties of the material. One of the ways to determine the effective properties could be the up-scale homogenization.

Homogenization methods are used for the computation of effective properties of a heterogeneous material, especially composites, based on the knowledge of the structural composition and material properties of all constituents. The wood is a natural cell-type

composite in which the cell walls are composed of fibre reinforced laminas. The cell structure itself strengthens the whole structure geometrically. Even the structural composition on a higher scale, i.e. arrangement of growth rings, resembles a laminate. Therefore, it is appropriate to use homogenization techniques for the computation of effective properties of wood. However, the wood composition and material properties of individual constituents evinces a great variability. Hence, the main tasks of this thesis are:

- Evaluation of wood structural composition and implementation of individual components into the computational model.
- Determination of the material properties of wood and its constituents.
- Experimental determination of wood properties, namely the density, moisture content, volume fractions of growth rings and pores, modulus of elasticity from the axial tensile test, indentation moduli of the cell wall, diffusion coefficient.
- Utilization of the homogenization methods for the determination of effective material properties and their comparison with values obtained by the measurements or taken from literature.
- Sensitivity of the results from homogenization to changes in inputs
- Determination of the microfibril angle (MFA) using homogenization and nanoindentation.
- Determination of the hygroexpansion coefficients.
- Comparison of the analytical and numerical homogenization.

The tasks are elaborated in individual chapters as follows. The spruce wood as a natural material is introduced in Chapter 2. The structural composition is described from the macroscale discernible by naked eye to the basic constituents of molecular base. Fundamental components are presented, together with the variability of wood structure caused by many factors. Chapter 3 describes the basic material properties of the wood such as mechanical (Section 3.2), moisture (Section 3.3) and thermal (Section 3.4). Probably, the most important quantity is the density, which is presented in Section 3.1 together with closely linked porosity. Some experimental results are mentioned in this chapter, which are further described in Chapter 5. The experimental section comprises e.g. determination of the density and moisture content, nanoindentation, image analysis, tensile tests etc. The theory of homogenization is elaborated in Chapter 4 including the employed homogenization methods. Subsequently, in Chapter 6 the homogenization

techniques are applied to wood to obtain the effective mechanical properties, moisture diffusion coefficients and coefficients of thermal conductivity considering the zero microfibril angle. The resulting effective properties are highly dependent on the chosen input parameters and assumptions, which is proved in Section 6.4, for the case of elasticity. The last chapter (Chapter 7) is dedicated to other applications of homogenization, such as the estimation of microfibril angle using the data from nanoindentation (Section 7.1) or the determination of coefficients of hygroexpansion (Section 7.2) provided by two different homogenization approaches. Section 7.2 presents different homogenization procedure than in previous chapters, where the analytical homogenization based on Mori-Tanaka method (Section 7.2.1) with different input values and assumptions and numerical approach (Section 7.2.2) up to level of lumens are introduced. At the end of this section, the comparison of both approaches is made in Tab. 25. The thesis is concluded with Chapter 8 summarizing all the acquired knowledge.

2 Wood composition

Generally, trees are woody plants with three principal parts: roots, single main stem (or trunk), and crown (comprising branches and leaves or needles). The stem is the main supporting part of the plant body, including its strength and dimensions, this determines it for use as a building element. The main task of the tree stem is not only the supporting one, but also it acts as a storage of manufactured organic substances and a conductor of water and nutrients. In the following, only the characteristics of the tree stem will be considered. The wood as a timber is further divided into softwoods and hardwoods. The Norway spruce (*Picea abies*) belongs to the conifers – a subclass of gymnosperms, and its wood belongs to the group of softwoods.

2.1 Macrostructure

Firstly, it is important to define three main directions of a timber: radial direction – from the centre of the stem to the periphery; tangential direction – in the direction of the tangent to growth rings; longitudinal or axial direction – along the stem. In connection to the basic directions, it is also necessary to define three types of sections: cross section – cut perpendicular to the direction of growth; radial section – in the radial direction, running through the centre of the stem; tangential section – in the tangential direction [2]. All these sections and directions are shown in Fig. 1.

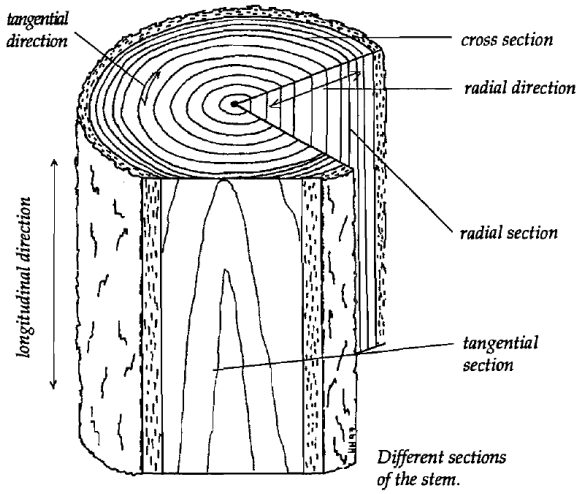

Fig. 1 Types of directions and sections in wood stem. [2]

The macrostructure of the wood in the cross section is discernible by naked eye. The stem is composed of several components present in concentric bands. The outermost

part is the outer bark, which protects the inner bark and xylem (an actual mass of the wood) against injuries, microbial attacks and other harmful agents. The inner bark transports sugars produced by photosynthesis from the leaves to the roots. The layer between bark and xylem is called vascular cambium and produces both adjacent tissues, where the growth occurs both outwards to widen the stem and upwards to make the tree taller. The xylem divides into sapwood, which is the living part of the wood and conducts water from the roots to the leaves, and heartwood differing in colour containing dead cells with accumulated organic compounds. The pith is in the centre of the tree stem and originated at the very beginning of the growth. A few rings in the middle of the stem are also called juvenile wood, which is dated to the time, when the tree was a small sapling [3]. The macrostructure composition is depicted on Fig. 2.

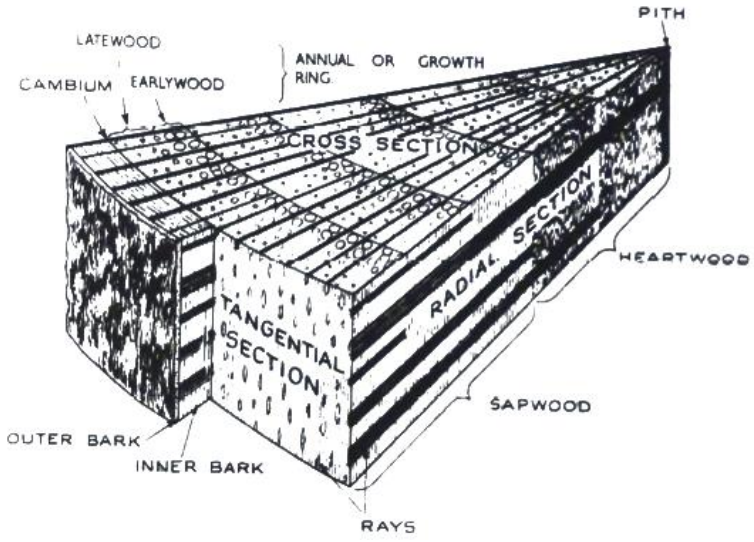

Fig. 2 Wood macrostructure. [4]

As it was mentioned, the cambium produces wood cells in layers to both sides – xylem and bark. The xylem layer formed during one growing season is called growth ring or annual ring. Each ring consists of two other layers, with more or less visible border. The lighter one is earlywood and the darker one is latewood. The layer of the earlywood is usually thicker than that of the latewood. Also, cells are bigger with thinner cell walls. The difference between both layers is caused by variance of the conditions during the growing season. At the beginning, it is necessary to transport as much water and nutrients as possible, so cells are bigger with large lumens and thinner walls, and increments of wood mass are very large, while at the end of the season the growth is slowing down and the main task changes into forming the support of the whole tree and storing nutrients. So, the latewood cell walls are much thicker, with very thin lumens, and the density is

higher. The width of the whole growth ring depends strongly on the kind of a tree and the growth conditions, such as temperature distribution during the season, precipitation amount, growth place etc. The growth rate slows down due to the low temperature, subsequently the growth rings become thinner and the density higher. This predetermines the wood from northern parts as a material with better mechanical properties compared to the wood from southern parts [5].

2.2 Microstructure

Wood, as well as other materials of biological origin, is made up of cells. New cells are produced in a cambium, this process is called the cell differentiation and lasts for three weeks, approximately [4]. In the case of softwood of conifers, only two types of the cells are present – tracheids and parenchyma cells. The major part of the spruce wood is comprised of the tracheids, approximately 94% of the total volume [5]. The microstructure, described below, is apparent on Fig. 3 and Fig. 4.

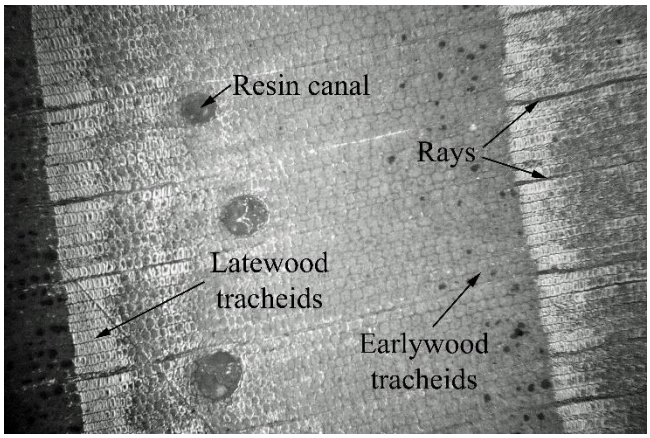

Fig. 3 Microstructure of the spruce (optical microscope) – cross section

Tracheids are long closed tube-like cells, with almost rectangular cross section, converging on their tips, oriented mainly longitudinally. The cavity inside the cell is called lumen, mainly used for transport of water and nutrients in the sapwood, while it is usually filled with extractives and other organic compounds in the heartwood. They are joined to one another finger like in the longitudinal direction and in the radial and tangential direction they are bonded by middle lamella, which acts as a ‘glue’ between cells. Continual flow through cells is enabled by pit pairs, possibly described as small holes in the cell wall at each end of the cell, see Fig. 5. The average length of spruce cell is about 2.5 – 2.82 mm. [5] According to Tsoumis [6] the mean cell length of axial

tracheids is 3.6 mm. The diameter of the tracheid varies for earlywood and latewood and depends on the direction, see Tab. 1.

Tab. 1 The diameters of tracheids in spruce [5]

Tangential direction		Radial direction	
Earlywood	Latewood	Earlywood	Latewood
32.7 μm	32.1 μm	39.3 μm	13.1 μm

It follows from the table that earlywood tracheids are almost square in shape, whereas latewood tracheids are rather rectangular with side ratio about 3:1. Another difference between earlywood and latewood is the cell wall thickness. In the first case, it is 1.5 μm and in the second one 5 μm [5]. Also, the number of pits is different for both types – 50 pits per radial wall in earlywood, in contrary to 15 pits in latewood; the same for pit diameters – 16.4 μm in earlywood and 6.1 μm in latewood [6]. The reason of this variation is obvious, both types have different purposes as it was mentioned in the previous section. In addition to the longitudinal direction, tracheids exist also in the radial direction in rays and their normal length is the same as parenchyma cells of the ray [5].

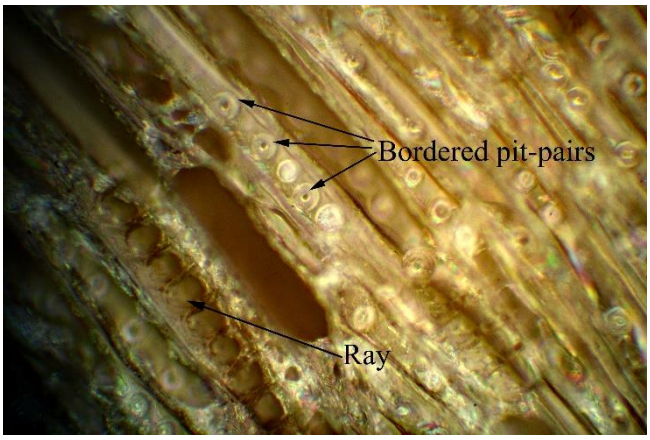

Fig. 4 Microstructure of the spruce (optical microscope) – tangential section

Another cell type are parenchyma cells appearing in axial as well as in radial directions. In the case of spruce, the axial parenchyma may be entirely absent. They are almost the same as tracheids, except that they are shorter, their shape is prismatic (brick-like) and have a different type of pits (simple). Their length is about 0.1-0.22 mm, with widths in a range of 0.01-0.05 mm [6]. Together with tracheids, the parenchyma cells form the basic structure of rays. They also appear in resin canals as supporting structural cells and gland cells (epithelium cells) secreting resin [5].

The next structural tissue is ray. It is composed of tracheids and parenchyma cells, running in the radial direction, i.e. from the pith to the bark. These structures provide nutrient transport in the radial direction. In the case of spruce, they appear as one cell wide and few cells high rows, see Fig. 4. The volume fraction of rays is about 5.9%, approximately [5].

Passage of water and nutrients between all types of cells are by way of pits. There are three forms of pits: bordered, semi-bordered and simple. Between two tracheids there are bordered pits, which occur predominantly on the radial walls. In the earlywood, there are more pits and they are bigger in size than that in the latewood. The bordered pit comprises secondary wall in the shape of 'saucers' on both tracheids with a hole in the centre. In the middle of these, there is a thickened part called torus connected to the edges by margo strands, which look like a net. The torus is pulled to one side during the process of wood drying, and more or less plugs the hole in the adjacent cell wall. This causes the reduction of permeability and the state is referred to as aspirated. The aspirated pits mainly occur in heartwood. The simple pits are predominantly between two parenchyma cells or a parenchyma cell and a tracheid. This type of pit comprises a cylindrical opening through the two adjacent secondary walls, while the primary wall remains as a semi permeable membrane [4].

Resin canals, also called resin ducts, are hollow tubes (cavities) surrounded by parenchyma cells (epithelial cells), which secrete resin into the canals. These canals appear in both directions – longitudinally and radially. In the spruce wood, the epithelial cells are thick walled. The resin canals arranged in the tangential direction are the result of wounding of the tree. These canals are called traumatic resin canals [4]. The volume fraction of the resin canals in spruce is about 0.14 % [5].

2.3 Ultrastructure

Wood can also be described as a natural fibre-reinforced polymer composite. Particularly, the cell wall could be considered as a multilayer laminate, where each lamella corresponds to one layer. Furthermore, each layer could be described as a fibre reinforced composite. There are small deviations between various cell types. In the following, the ultrastructure composition of the tracheid will be described.

The basic division of individual layers are depicted on Fig. 5. Describing outwards, the layers are: warty layer, secondary wall, primary wall and middle lamella (sometimes

called intercellular layer). The middle lamella does not exactly belong to the cell wall layers, but joins two adjacent cell walls together. It forms in the same time as a primary wall. It is totally amorphous and appears to be continuous and homogeneous. The middle lamella is probably the weakest microstructural part compared to the cell wall. The outermost cell wall layer is a primary wall, which is the first produced part of the cell wall during cell division in the cambium. Maybe, that is the reason of the imperfection of this layer. The primary wall is very thin and elastic so the forming cell can expand to its final size. Microfibrils are arranged randomly in this layer [5]. Attached to the primary wall is the major part of the cell wall – secondary wall. Further it subdivides into three layers – S_1 – the outer layer, S_2 – the middle layer and S_3 – the inner layer. These layers are organized in a plywood type of construction. The S_1 and S_3 are relatively thin, with a large microfibril angle (microfibrils will be mentioned later), defined as the deviation of the microfibrils from the longitudinal axis. The S_1 layer is composed of several lamellae with a crossed fibrillar texture, which means that the orientation of microfibrils is alternating in each lamella [7]. It takes about 10-15% of the total thickness of the secondary wall [5].

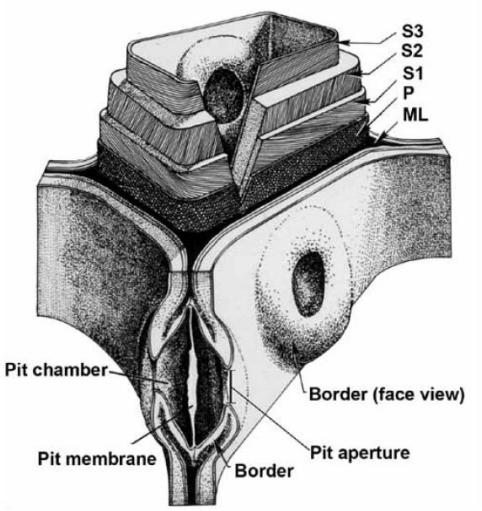

Fig. 5 Structure of the tracheid

ML – Middle lamella; P – Primary wall; S_1 – Outer layer; S_2 – Middle layer; S_3 – Inner layer [3]

The most important part, with a great impact on final properties, is probably the middle layer. The middle layer is covering about 85% of the secondary wall total thickness. The microfibrils inside are parallel to each other and are running spirally along the longitudinal axis. The MFA (microfibril angle) of the middle layer is about 0° - 30° [4]. The innermost secondary wall layer is the inner layer – S_3, with the same composition as the outer layer, but the angle from axial direction is higher. The inner layer covers

about 5% of the total thickness of the secondary wall. However, it could be absent in some species. A continuous thin amorphous layer called a warty layer and containing some fibres and warts is attached to the inner layer. It could be also missing in some species [5].

Wood is like other biological materials a carbohydrate, comprising three basic chemical elements: carbon, hydrogen and oxygen in the ratios of 1:2:1 [8]. The wood cell walls consist mainly of cellulose (predominantly crystalline), hemicellulose (predominantly amorphous) and lignin (totally amorphous). Apart from these basic components, other substances appear in the wood microstructure, such as extractives, water and some additional minor components.

The most important constituent of wood is the cellulose ($C_6H_{10}O_5$) – a semi-crystalline thermoplastic natural polymer forming the reinforcing microfibres in the cell wall. It is produced by polymerization of glucose monomers into a linear molecule chain. The molecule chains can form larger units, with alternating crystalline (predominantly) and amorphous regions [5]. The cellulose units are parallel to each other in highly ordered chains in the crystalline regions. These areas do not absorb water in comparison with non-crystalline regions that also alter the properties of microfibril [8].

Hemicelluloses are heteropolysaccharides composed of glucose and other monomers, such as mannose, galactose, xylose, arabinose etc. Polymerization degree of the hemicelluloses is low. The structure is semi-crystalline, similar to cellulose, but with dominant amorphous sections [5]. The hydrogen bonding connects hemicellulose chains together or with cellulose chains. It exhibits high moisture adsorption capacity [8].

The last basic constituent is lignin. It is completely amorphous and has large three-dimensional molecular structure, which is chemically very complicated and heterogeneous [8]. There are many types of lignin differing due to its location. The main task of lignin is to act as a ‘glue’ between macro fibrils (the units composed of cellulose microfibrils and the hemicellulose layer around them) as well as between cell walls. Furthermore, it protects the cellulose and hemicellulose from the detrimental influence of water because of its hydrophobic nature [5]. The lignin begins to soften at about 170°C [8].

The generally accepted model of the microfibril is that with the length considered as indefinite and with the rectangular cross section (about 10x5 nm). It consists of

a crystalline core comprising cellulose molecular chains, surrounded by low crystallinity area comprising amorphous cellulose and hemicellulose. These threads are bonded together by lignin [4]. As it was mentioned in the previous sections, the microfibrils are probably responsible for the strength deviations among every single timber of the same species. Particularly, it depends on the microfibril angle, where the lower angle corresponds to higher strength. So, the examination of the MFA-strength dependence can help to determine mechanical properties of the wood.

2.4 Variation of wood structure and structural defects

A great disadvantage of wood is probably its variability. It is very unlikely that two pieces of timber are of the same appearance and properties. The variability is caused by many factors. These factors could be divided into four basic groups: genetical causes, systematic variability, environmental reasons and presence of defects [4].

The difference between various families is certain, but there are differences even amongst the trees of the same species growing next to each other, all caused by genetics. Variability due to systematic sources is additional to that of genetics and appears within a tree both horizontally (from pith to bark) and vertically (from base to top). In the direction from pith to bark structural characteristics vary due to age (juvenile, mature and overmature wood), growth ring structure, cell morphology (cell length, wall thickness, cell and lumen dimensions), ultrastructure (microfibril angle, degree of crystallinity) and chemical composition (lignin and cellulose content). In the vertical directions, changes appear similarly as in the horizontal. Another important factor is the formation of heartwood – the difference between sapwood and heartwood was already mentioned [6].

Any environmental factor that affects the growth of the tree will influence the wood structure and its properties. These factors are for example moisture, nutrients in the soil, light, temperature, wind, growth rate (faster growing are usually weaker), tree spacing, changes of the tree shape (pruning) etc. [6].

Naturally, the tree grows vertically, it is almost cylindrical in shape with circular cross section. Exposure to some environmental factors, such as wind, causes deviations from the ideal shape. In many cases, reaction wood can develop. The reaction wood is a response to loading of the tree and appears in three forms: tension wood, compression wood and contrasting wood. The tension wood develops only in deciduous trees in areas under tensile stress, usually on windward side. On the other hand, the compression wood

could be found only in conifers in places under compression (leeward side). Both cases provoke widening of growth rings, changes in colour (compression wood is darker in tone, tension wood is lighter than normal wood), cell structure and chemical composition (cell shape, cellulose and lignin content). Contrasting wood develop on the opposite side to the reaction wood [5].

An important growth feature is a spiral grain. It occurs when longitudinal cells run helically around the stem. After the bark removal, it is possible to see the twisted appearance of the stem caused by it. There are two patterns in softwoods: the first one starts as left-handed near the pith, then changes to straight and finally to right-handed spiral pattern. The second one is left-handed spiral that keeps developing all the time [8].

The last-mentioned growth feature will be a knot. The knot is an inclusion of the basal part of a branch within the stem. There are two types of knots depending on its origin. If the branch is alive during its inclusion, its surrounding is connected and give rise to intergrown or tight knot. On the other hand, an encased or loose knot is formed after the branch died and may fall off during drying. Knots have adverse effect on the appearance and properties of wood. They act as discontinuities in the wood mass. There are grain deviations around them and if the wood is under load, it is the source of the crack initiation [6].

There are many other natural defects such as bark pockets, resin streaks etc., which have not been mentioned, see, e.g. [4] for more information.

It is important to mention the growth stress which may cause degradation of wood. In some species, the stresses are so intense that trees, when felled, split apart [6].

3 Wood properties

Various important wood properties are described in the following chapter. Example values taken from the literature are stated in each section to provide basic overview to the reader. In some sections examples of the experimental results are presented, referring to Chapter 5. The first section is concerned with the description of different types of the density and determination of the porosity, with division into individual phases. Probably the most important is the Section 3.2 discussing the mechanical properties of the wood. This section is followed by moisture properties focused on the determination of the moisture content and moisture diffusion coefficient. The last section describes thermal properties, mainly the thermal conductivity.

3.1 Density and porosity

Density is a key quantity of wood, which correlates with most mechanical properties. Basically, it is defined as a ratio of mass to volume:

$$\rho = \frac{m}{V} \left[\frac{kg}{m^3}\right] \tag{3.1}$$

where m is the mass [kg] and V the volume [m^3] of the wood piece.

There are many factors affecting the density. The main factor is the moisture content, because wood is hygroscopic material and attracts water very much. The moisture adsorption increases both the weight and volume of the wood. According to conditions during measurement, there are various types of density values [5]:

Dry density (oven-dry density) (ρ_{dry}) means the ratio of mass to volume both measured in the oven-dry state, i.e. heat-treated for a period of 12-48 h at the temperature of 103±2°C.

Green density (ρ_{green}) means that the measurement is carried in a "green" condition, i.e. the moisture content is at or over the fibre saturation point (FSP).

Air-dry density is the value measured on air-dry wood, i.e. it has been dried at room temperature and the moisture content is about 12%.

Dry-green density is defined for mass measured for oven-dry wood and volume for the wood in the green condition.

Density of wood substance (*density of cell wall*) (ρ_{cw}) corresponds to the density of cell wall itself (without influence of dissolved water).

Basic density is similar to dry-green density, where the volume is measured in the condition with lumens full of water (i.e. the volume is at its maximum).

Some example values taken from literature are listed in Tab. 2. In the range of 0 and 25% moisture content, the density can be calculated as [6]:

$$\rho_{wet} = \rho_{dry} \frac{1 + u}{1 + 0.84\, \rho_{dry} u} \tag{3.2}$$

where ρ_{dry} is the oven-dry density [g/cm^3], u is the moisture content [-] and ρ_{wet} is the density at the corresponding moisture content.

Tab. 2 *Density of Norway spruce (Picea abies)*

Density [kg/m^3]		
Dry	Dry-green	Air-dry
410[1]	376[2]	320-550[1]
	370[2,a]	
	382[2,b]	

[1] Tsoumis [6], *[2] Kettunen* [5] *([a] forest, [b] ridge)*

As it was mentioned above, wood is a porous material and the porosity strongly affects the resulting values of density. The density of wood is therefore given as an amount of cell wall material contained in a certain volume. Reversibly, it is possible to compute the volume fraction of pores using the known wood density and the density of the cell wall material. Considering that the only one type of pores are lumens, its volume fraction could be derived as [6]:

$$f_{lum} = \left(1 - \frac{\rho_{dry}}{\rho_{cw}}\right) \tag{3.3}$$

where ρ_{dry} is oven-dry density [kg/m^3] and ρ_{cw} is density of the cell wall material [kg/m^3]. Variation of the density depends on factors mentioned in Section 2.4, such as cell wall thickness, lumen size and its distribution in the whole tree, deposition of extractives,

etc. The variability is evident between different species, trees of the same species and even in different areas within a tree.

The determination of wood porosity is crucial for further examination of the wood properties. Maybe the easiest way is the application of Eq. (3.3) for measured dry density of the wood and cell wall density set equal to 1500 kg/m^3 [5] considering that the cell wall has the same properties independent of the tree species. However, this approach gives the overall porosity without any differentiation between earlywood and latewood. In [9] the authors provide more accurate computation of the cell wall density based on known weight fractions and densities of the cell wall constituents and a variable moisture content of the cell wall. The density of wet cell wall is then given by [9]:

$$\rho_{cw}^{wet} = \left(\sum_{s=1}^{n} \frac{WF_s^{wet}}{\rho_s} \right)^{-1} \tag{3.4}$$

where WF_s^{wet} is the weight fraction of the wet constituent [-], ρ_s is the constituent density [g/cm^3] and $s \in \{$*crystalline cellulose, amorphous cellulose, hemicellulose, lignin, extractives, water*$\}$. Recalling Eq. (3.3), the volume fraction of lumens in the earlywood and latewood could be computed by substituting ρ_{dry} with ρ_{ew}^{wet} or ρ_{lw}^{wet}. The mass density of the dry earlywood and latewood could be computed from:

$$\rho_{ew}^{dry} = \frac{\rho_{dry}}{f_{ew} + f_{lw} \left(\frac{\rho_{lw}}{\rho_{ew}} \right)^{dry}};\ \rho_{lw}^{dry} = \rho_{ew}^{dry} \left(\frac{\rho_{lw}}{\rho_{ew}} \right)^{dry} \tag{3.5}$$

where ρ_{dry} is oven-dry density [kg/m^3], $\left(\frac{\rho_{lw}}{\rho_{ew}} \right)^{dry} = 2.6$ is given for spruce according to [10] and the volume fractions of earlywood and latewood could be derived from:

$$f_{lw} = 3.75\, \rho_{dry} - 1.27; f_{ew} = 1 - f_{lw} \tag{3.6}$$

where the oven-dry wood density is within the range of 339-605 kg/m^3 [10]. The mass density of the wet earlywood ρ_{ew}^{wet} and latewood ρ_{lw}^{wet} could be computed employing Eq. (3.2) for a given moisture content *u*.

Example values of the computed volume fractions are summarized in Tab. 3 using the moisture content and dry wood density of data set containing five samples. The derivation of the moisture content and densities is further described in Section 5.1. The

volume fractions of the earlywood and latewood (f_{ew} and f_{lw}) were computed employing Eqns. (3.6). Using these values, it is possible to calculate earlywood and latewood densities by Eq. (3.5). With a knowledge of the cell wall density obtained by Eq. (3.4), the volume fractions of lumens could be derived from Eq. (3.3). The moisture content could be accounted for by Eq. (3.2).

Tab. 3 Measured dry wood densities with corresponding volume fractions, see Section 5.1

No	u	ρ_{cw}^{wet}	ρ_{dry}	f_{ew}	f_{lw}	f_{lum}^{ew}	f_{lum}^{lw}	f_{lum}	
	[-]	[kg/m^3]	[kg/m^3]	[-]	[-]	[-]	[-]	(1)	(2)
2	0.046	1430.04	450.62	0.580	0.420	0.805	0.501	0.677	0.685
6	0.042	1431.14	492.83	0.422	0.578	0.815	0.527	0.648	0.656
11	0.040	1431.60	432.42	0.648	0.352	0.801	0.490	0.691	0.698
15	0.034	1433.04	510.23	0.357	0.643	0.820	0.537	0.638	0.644
38	0.041	1431.43	429.38	0.660	0.340	0.800	0.487	0.693	0.700

The values in the last two columns were obtained by two methods. The data in the column (1) were computed using simple weight arithmetic mean of values from the columns on the left hand side of this column, i.e. $f_{lum} = f_{ew} f_{lum}^{ew} + f_{lw} f_{lum}^{lw}$. The values in the column (2) were obtained employing Eq. (3.3). Comparing both approaches the resulting volume fraction of pores is quite similar.

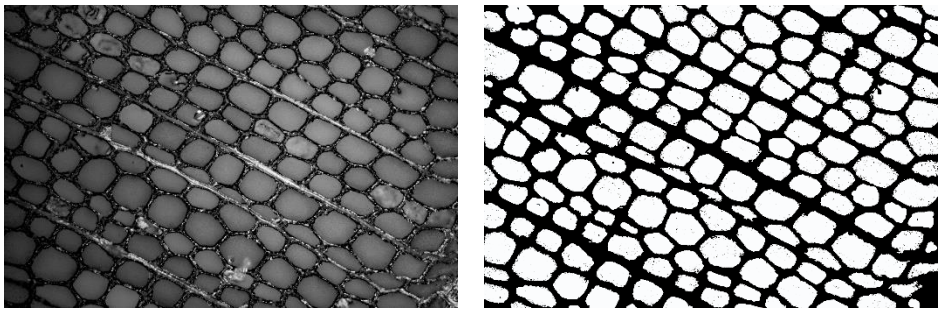

Fig. 6 SEM image of spruce earlywood: Original greyscale image (left) and binary image (right)

Better view of the wood microstructural composition can be provided by image analysis, see also Section 5.3. Basically, the image analysis is based on capturing image by using different types of microscopy and evaluation of the volume fractions of areas with different colours, usually by a programme. It could be helpful to transform the image to binary, where one colour corresponds to pores and the second one to a solid phase. An example is depicted on the Fig. 6 (white=lumens, black=cell wall).

An advantage of this approach is the direct view of microstructure with all its inhomogeneities and defects. Also, it is possible to differentiate earlywood and latewood tracheids and other constituents, such as rays and resin canals. However, it provides information only about one cross section and we have no idea about material in the direction perpendicular to the surface, which can lead to great errors. On the other hand, the evaluation is very simple and images taken by basic optical microscopes are satisfactory. Problems could be caused by a sample preparation, where a chosen technique can affect the resulting image and so the values of lumen volume fractions. As an example, the conventional scanning electron microscope (SEM) operates under high vacuum, which leads to the removal of air from pores and therefore to the cell contraction.

More information about wood structure can be obtained by X-ray microtomography [11], which provides a 3D image of the structural composition. This method is considerably more demanding in the amount of data to be processed in comparison to 2D image analysis. An example of reconstructed structural composition of spruce is depicted on Fig. 7. The reconstructed 3D image (CT-scan) can be sliced digitally in any desired plane for further analysis. This method does not require any special sample preparation, therefore many factors influencing the change of internal structure are eliminated.

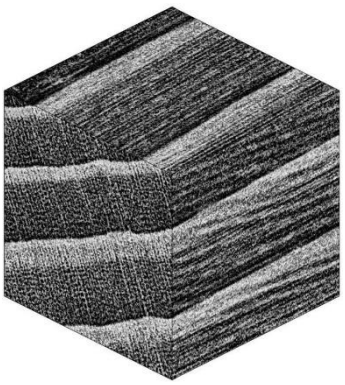

Fig. 7 Reconstructed 3D image from single source double-energy method [12]

Previously mentioned methods are compared in Tab. 4 for spruce samples. The values in a row ‘Density’ were computed employing Eqns. (3.3) and (3.6) with mean values of the measured dry wood density $\rho_{dry} = 422.73$ kg/m^3 and the moisture content u=4.50%, respectively. The values of the image analysis method were obtained by measurements of 58 samples in the case of growth rings and of six samples in the case of lumens. It is important to point out that the values from CT scan were obtained for

a different sample, whereas the first two mentioned methods are for the samples with the same origin.

Tab. 4 Comparison of methods for evaluation of volume fractions

	f_{lum}^{ew}	f_{lum}^{lw}	f_{ew}	f_{lw}
Density	0.80	0.48	0.68	0.32
Image analysis	0.69	0.12	0.80	0.20
CT scan	0.75	0.20		

All mentioned methods give more or less similar estimates of the volume fractions of lumens in the earlywood, whereas the value corresponding to the latewood lumens computed from density is overestimated, see Section 5.3. The volume fractions of the earlywood and latewood are reasonable for first two methods. It is necessary to emphasize that reasonable values computed by Eq. (3.6) are obtained only in the middle of the mentioned interval, whereas the resulting values at the margin of the interval could be considered as less credible. An inappropriate derivation of the volume fractions employing previously mentioned equations and validation of this claim is further proved in Section 5.2 and 5.3.

3.2 Mechanical properties

Mechanical properties represent ability of material to resist the applied external forces, depending on their magnitude and a manner of loading (tension, compression, shear, bending etc.). Wood behaviour differs in growth directions, i.e. it is mechanically anisotropic. Main differences are between longitudinal (axial) direction and transverse (radial and tangential) direction, due to its cellular structure and direction of the reinforcing fibres. From that, it resembles the behaviour of synthetic fibre-reinforced thermoplastics in combination with the cell structure.

Basically, the material behaviour is obtained from the stress-strain relation. Under increasing load, the deformation is reversible, i.e. loading and unloading follows the same straight-line starting in zero, until it reaches the limit of proportionality. Above this point the permanent deformation occurs. Increasing load will result in more permanent deformation and finally in failure. The stress level at which failure occurs is considered as strength depending on the manner of load. It is important to mention that wood evinces

anelastic (viscoelastic) behaviour, i.e. the strain is partially proportional to the applied stress and also partially to viscosity and duration of loading.

Tab. 5 Typical values of stiffness coefficients of spruce at 12% moisture content [13]

E_L [MPa]	E_R [MPa]	E_T [MPa]	G_{LR} [MPa]	G_{LT} [MPa]	G_{RT} [MPa]	ν_{RL} [-]	ν_{TL} [-]	ν_{TR} [-]
13500-16700	700-900	400-650	620-720	500-850	29-39	0.018-0.030	0.013-0.021	0.240-0.330

Elastic behaviour of wood can be characterized by a set of twelve constants (nine are independent), namely three moduli of elasticity *E* (MOE), three shear moduli *G* and six Poisson's ratios *v*. Modulus of elasticity *E* [$N/mm^2=MPa$], also called Young's modulus, is in simplified way defined as the slope of the tensile stress-strain curve in the elastic deformation region. The shear modulus *G* [$N/mm^2=MPa$] indicates the resistance of a member to shear stress. During loading the deformation occurs both parallel and perpendicularly to the load direction, where the latter one is proportional to the first mentioned. The ratio of the transverse to axial strain is called Poisson's ratio and is denoted by *v* [-]. Assuming orthotropic material and the validity of Hooke's law, these constants can be overwritten into the form of compliance matrix:

$$\mathbf{M}=\begin{vmatrix} \frac{1}{E_R} & -\frac{\nu_{TR}}{E_T} & -\frac{\nu_{LR}}{E_L} & 0 & 0 & 0 \\ -\frac{\nu_{RT}}{E_R} & \frac{1}{E_T} & -\frac{\nu_{LT}}{E_L} & 0 & 0 & 0 \\ -\frac{\nu_{RL}}{E_R} & -\frac{\nu_{TL}}{E_T} & \frac{1}{E_L} & 0 & 0 & 0 \\ 0 & 0 & 0 & \frac{1}{G_{LT}} & 0 & 0 \\ 0 & 0 & 0 & 0 & \frac{1}{G_{LR}} & 0 \\ 0 & 0 & 0 & 0 & 0 & \frac{1}{G_{RT}} \end{vmatrix} \tag{3.7}$$

where the three principal directions are the longitudinal direction L, the radial direction R and the tangential direction T, correspondingly to the wood structure (Fig. 1). Following the assumption of the linear elastic material, the compliance matrix is

symmetric and from that, there are nine independent parameters. The ranges of values of these parameters at a level of solid wood are summarized in Tab. 5.

Recalling Section 2.3 wood is composed of several materials with various material properties. Together with cellular structure the wood evinces variability of the material properties at different scales. As an example, the strength in axial tension of the solid wood is 50-60 MPa, whereas in transverse tension the strength lowers to values of 1-7 MPa. The axial strength of a single cell is considerably higher with a range of 200-1300 MPa. It could be expected that the cellulose chains considered as the main load-bearing constituents evince the highest values of about 7500 MPa [6].

Tab. 6 Mechanical properties of the cell wall constituents [9]

Phase	Bulk modulus $K\ [GPa]$	Shear modulus $G\ [GPa]$	Poisson's ratio $\nu\ [-]$
Hemicellulose	8.89	2.96	0.35
Lignin	5.00	2.30	0.30
Water + extractives	2.30	0.00	0.50
Amorphous cellulose	5.56	1.85	0.35
	Stiffness matrix elements (nonzero) $[GPa]$		
Crystalline cellulose	$L_{11} = L_{22} = 34.86; L_{33} = 167.79$ $L_{44} = L_{55} = 5.81; L_{66} = 4.53$		

The knowledge of the properties of the material at lower scales is very important at least to understand the material behaviour. Furthermore, it is possible to determine the properties of the solid wood employing homogenization techniques. The computation will be described in the Chapter 6. To that end, it is necessary to introduce the mechanical properties of the cell wall constituents, see Tab. 6. The phases in the upper block of the table are considered as isotropic materials, while the crystalline cellulose is approximated by transversely isotropic material with zero off-diagonal elements, i.e. the Poisson effects and coupling between shear and normal stress are neglected according to [9]. However, the veracity of these values is not certain, mainly because of complicated measurements of individual constituents. Even the material behaviour of each constituent can be considered differently in various studies. The presented mechanical properties are considered as moisture independent, whereas in [13] the author proclaims the dependency

of the hemicellulose and lignin on the moisture content. Also, the hemicellulose is described as the transversely isotropic material according to this author, while it is considered as isotropic in this thesis.

Besides the mechanical behaviour, the proper structural design can not be done without the knowledge of the strength of the material. Strength of wood could not be characterized by one value, but is divided depending on the manner of loading. The basic types of strength are compression, tensile, bending and shear, each of them further divided into values parallel and perpendicular to the grain, respectively. In addition, there are more values characterizing mechanical properties of the wood such as cleavage, toughness, hardness, torsion, fracture and fatigue that are not included in this thesis, the reader is referred to the literature e.g. [4; 5; 8] for more information.

Tab. 7 Modulus of elasticity in axial tension of Norway spruce, see Section 5.4

Sample	ρ_{dry} [kg/m^3]	MC [%]	E [GPa]	Peak stress [MPa]
2	450.62	4.62	15.31	70.3
6	492.83	4.19	10.91	87.6
11	432.42	4.00	16.25	67.7
15	510.23	3.40	16.01	68.4
38	429.38	4.07	13.14	44.5

Wooden elements in structures are mostly placed horizontally as beams and their mode of deflection is primarily bending. The static bending is also the most used test method for the determination of mechanical properties. This test provides the bending strength, usually presented as a modulus of rupture (MOR), which corresponds to the stress in extreme fibres at a point of failure, if the simple bending theory is assumed. From the elastic part of the load-deflection graph, it is possible to determine the modulus of elasticity. More accurate values of the MOE could be obtained by the axial tension tests, together with strength in axial tension and contraction, which leads to Poisson's ratios. An example of measured values of the modulus of elasticity in axial tension are listed in Tab. 7. The tensile tests are further described in Section 5.4. In the case of vertical members, such as columns, the value of the strength in compression is needed. The strength in compression is about half of that in tension [6] and is often affected by

buckling. Another important value is the strength in shear, where the values of the axial shear are lower than that of transverse shear, due to the wood structure.

The mechanical properties are influenced by many factors. As it is evident from the previous paragraph and Tab. 8, the values change with different manner of loading and the loading direction. In most cases, an increasing deviation from the longitudinal direction causes the reduction of the strength values, e.g. the ratio of longitudinal to the horizontal value of tensile strength and stiffness is about 40:1 [4]. This change among directions is caused by the cellular structure of the wood and the deviation from the longitudinal direction of the reinforcing fibres in the S_2 layer. The structure appears stronger under the axial tension than the corresponding compact structure. This phenomenon is called a geometric strengthening, whereas in the axial compression the deformation is larger [5]. The measured values depend on the size of the tested sample, where the ratio of bending : tension : compression strength of the small clear sample is 6:9:3, whereas the same ratio of the structural-sized sample is 6:4:4 [4]. This difference is mainly due to absence of the defects (e.g. knots, pitch pockets, bird pecks) in the clear wood sample. Another natural factors affecting mechanical properties even of the clear wood samples are grain deviations, checks, presence of the reaction or juvenile wood, growth ring orientation, extractive content, compression failures, etc. Also, the loading rate (i.e. how fast is the load applied) and the duration of the load change the resulting values.

Tab. 8 Strength of spruce wood for different types of loading with corresponding MOE

Tension		Compression		Static bending		Shear	
∥	⊥	∥	⊥	MOR	MOE		
84	1.5	30	4.1	60	9100	5.3	1)
104	-	36.5	-	72	10200	9.8	2)

1) *Tsoumis* [6], 2) *Desch and Dinwoodie* [4]

All values are in [MPa]

The most significant factor of the environment is probably the moisture content. Its effect is significant when the moisture content is below the FSP, whereas changes appear rather slightly above the FSP. Magnitude of the moisture influence is different for different properties. Another environmental factor is temperature. In general, the strength properties decrease with increasing temperature. However, the influence of the

temperature is simultaneously affected by changing the moisture content. Similar to loading, the exposure to high temperatures for a long term results in a marked reduction of the strength, stiffness and toughness. Due to chemical decomposition of wood, very high temperatures (above 200°C) will reduce the strength in few minutes. These were the basic factors influencing the mechanical properties, nevertheless many other exist.

3.3 Moisture properties

The wood is naturally hygroscopic material. It means that it attracts moisture from the surrounding atmosphere and holds it in the form of liquid water or water vapour. The water conduction and inherent moisture content are very important, because it affects all other properties.

In a living tree, the motion of liquids is upwards in the sapwood of xylem and downwards in the inner bark. There are two types of motion obeying the Fick's first law: flow along lumens, driven by difference of pressures, and diffusion along lumens or through cell walls dependent on a concentration gradient. The surface energy between the cell wall and the liquid influences the capability of liquid to wet the surface of cell walls and to penetrate the cell wall structure. If the liquid wets the cell wall well, the surface of the liquid in the lumen becomes concave and tends to move upwards (acropetal flow). On the contrary, if the surface is convex, the flow motion is downwards (basipetal flow) and it identifies a poorly wet cell wall. This phenomenon is called capillary action or capillarity. The acropetal flow is supported by underpressure in the axial cells of the upper part of stem, which is caused by evaporation of the water from the foliage [5].

The basic quantity is a moisture content (MC), defined as a ratio of mass of water to oven-dried wood mass. The moisture enters the wood mass, because of attraction of water molecules by the hydroxyls of its chemical constituents. Moisture is present in wood in two forms: free water (i.e. liquid water or water vapour in lumens and cavities) and bound water (i.e. liquid water in the cell wall) [5]. The natural state of living tree is called green wood and the moisture content at this state can range from about 30% to more than 200% depending on wood species etc. [3]. In softwoods, the moisture content differs between sapwood and heartwood, because of presence of extractives, which cover the lumen surfaces and pits and cause a decrease in permeability [5]. In the case of Norway spruce the corresponding values of moisture content in green state are 40-50% for the heartwood and 160 % for the sapwood, respectively [6]. After the tree is cut down,

the wood starts to lose water, which is termed desorption. The reverse process is called adsorption and means water gain. If the wood is left under constant conditions of temperature and relative humidity of surroundings, the moisture retains a final quantity = equilibrium moisture content (EMC). The relationship between EMC and relative humidity at constant temperature is referred to as a sorption isotherm. The values obtained from desorption and from adsorption differ, where that from desorption are higher. Graphically it is expressed as a hysteresis loop, see Fig. 8, where a – initial desorption, *b* – adsorption, *c* – desorption following drying and saturation [6].

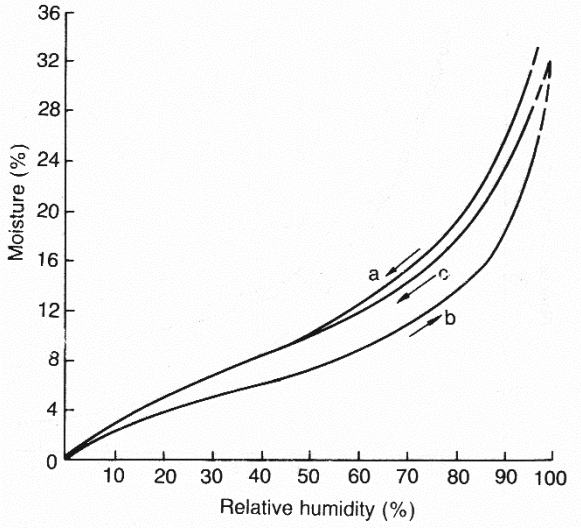

Fig. 8 Moisture sorption isotherms for linden (32°C) [6]

Decrease of the sorption isotherm *c* in comparison to a is caused by reduction of the wood permeability due to pit aspiration. The pit aspiration occurs during drying and it means that the membrane and its torus are aspirated to the pit aperture and pit becomes closed. If the closing period is longer, extractives glue the torus strongly to the aperture and to the wall of the bordered pit, the closing is irreversible [5].

When the cell walls are fully saturated and there is no free water, i.e. there is no water present in lumens, the state is called fibre saturation point (FSP) with average value of about 30% [3]. The values of the FSP for Norway spruce (*Picea abies*) are given for different temperatures as 29.3% (20°C), 23.7% (40°C) and 17.6% (65°C), according to [5]. This point is very important, because below the FSP, most properties change as a function of MC and so the dimensions. Dimensional changes further subdivide into shrinkage – changes that are results of the initial drying from green to dry conditions; and movement – changes that occur due to daily or seasonal changes in relative humidity of the atmosphere. The most significant shrinkage occurs in the tangential direction, almost

twice as high as that in the radial direction. Whereas in the longitudinal direction it is usually less than 0.1%. All values for both dimensional changes are measured in case of free movement. If the movement is not allowed, the wood becomes permanently or irreversibly compressed (=compression set) or tensed (=tension set) [4].

When both the cell walls and lumens are fully saturated, the corresponding moisture content reaches its maximum (=maximum moisture content) [3]. However, it could differ between various cycles of adsorption and desorption due to aspirated pits as it was mentioned earlier.

Basic method of moisture content determination is drying and weighing, where the wood sample is weighed before and after drying in an oven. The gravimetric moisture content of the sample is therefore [4]:

$$MC = \frac{m_{init} - m_{dry}}{m_{dry}} \times 100\ [\%] \tag{3.8}$$

where m_{init} $[g]$ is the initial mass of the sample and m_{dry} $[g]$ is oven-dry mass of the sample. It is important to mention that hot samples shouldn't be weighed, because it leads to smaller values than actual. And if the wood is kept in an oven too long, the gradual decomposition of chemicals will start [6]. An example of the determination of MC is shown in Tab. 9, where samples were left in an oven at temperature of 40°C for several days. See Section 5.1 for more details about the measurement.

Tab. 9 Measured masses and moisture content of the Norway spruce samples, see Section 5.1

Sample	m_{init} $[g]$	m_{dry} $[g]$	MC $[\%]$
2	1.63	1.56	4.62
6	1.17	1.12	4.19
11	1.22	1.17	4.00
15	1.66	1.61	3.40
38	1.33	1.28	4.07

However, this approach is not suitable for resinous samples, because much of the resin will be lost on drying and will be treated as water in the calculation. In this case, the distillation method could be better choice. Another type of the measurement is based on the change of electric properties with change of moisture, where devices are called

moisture meters and basic types are resistance meters, capacitance meters and power-loss meters [4].

The fibre saturation point is important for the determination of water motion. When the moisture content reaches or overrides the fibre saturation point, the flow of water appears in the cell wall and lumens. Whereas below the FSP the motion changes into diffusion [5]. The diffusion processes in wood involve the movement of bound water through the cell wall and the movement of water vapour through the lumen. In an environment, where the wood is used, the moisture concentration and temperature change with time and from that the transport processes are transient. It leads to the solution of the three coupled differential equations with strongly non-linear anisotropic material behaviour [14]. For the sake of simplicity, the steady-state conditions are considered, which means that fluxes and concentrations do not change with time and the two phases (bound water and water vapour) are in equilibrium [15]. The steady-state diffusion is described by Fick's first law of diffusion as follows [14]:

$$\mathbf{J} = -\mathbf{D}\frac{\partial c}{\partial \mathbf{x}} \tag{3.9}$$

where **J** is the macroscopic (effective) moisture flux, which is linked to the macroscopic concentration gradient $\partial c/\partial \mathbf{x}$ by the macroscopic (effective) diffusion matrix **D** Therefore the desired material property is the diffusion matrix. The orhotropic diffusion matrix of the cell wall material is given according to [15] as:

$$\mathbf{D}_{cw} = \begin{bmatrix} D_{cw,trans} & 0 & 0 \\ 0 & D_{cw,trans} & 0 \\ 0 & 0 & D_{cw,long} \end{bmatrix} \tag{3.10}$$

where the transverse diffusion coefficient of the cell wall $D_{cw,trans}$ [m^2/s] is defined as:

$$\begin{aligned} &D_{cw,trans} \\ &= 1.832\times10^{-4} \\ &\times \exp\left(-\frac{43623 - 20625\,u - 1227\,ln\,u}{RT}\right) \end{aligned} \tag{3.11}$$

with R = 8.314472 [*J/mol.K*] as the universal gas constant, T [K] as the actual temperature and u [-] as the moisture content. Finally, the longitudinal cell wall diffusivity $D_{cw,long}$ [m^2/s] is calculated as:

$$D_{cw,long} = 2.5\, D_{cw,trans} \tag{3.12}$$

The diffusion coefficient of water vapour in moist air D_{air} [m^2/s] occurring in the lumens is according to [15] given by:

$$D_{air} = 2.31{\times}10^{-5}\left(\frac{p_{atm}}{p_{atm}+p_v}\right)\left(\frac{T}{273.15}\right)^{1.81} \tag{3.13}$$

with T [K] denoting the actual temperature, p_{atm}=101 325 Pa as a sea level standard atmospheric pressure and the vapour pressure p_v defined as:

$$\begin{aligned} p_v = \varphi p_0 = \varphi \Big\{ & 2.2064{\times}10^7 \\ & \times \exp\Big[\frac{647.14}{T}(-7.85823\tau + 1.83991\tau^{1.5} \\ & - 11.7811\tau^3 + 22.6705\tau^{3.5} - 15.9393\tau^4 \\ & + 1.77516\tau^{7.5})\Big]\Big\} \end{aligned} \tag{3.14}$$

with τ given as:

$$\tau = 1 - \frac{T}{647.14} \tag{3.15}$$

where φ [-] is the relative humidity of the surrounding air and T [K] is the actual temperature. The diffusion of air in the lumen is written in the matrix form as:

$$\mathbf{D}_{lum} = D_{air}\mathbf{I} = \begin{bmatrix} D_{air} & 0 & 0 \\ 0 & D_{air} & 0 \\ 0 & 0 & D_{air} \end{bmatrix} \tag{3.16}$$

The diffusion matrices $\mathbf{D}_{cw}$ and $\mathbf{D}_{lum}$ are set as properties of initial phases used for the homogenization in Section 6.1.

The diffusion coefficient can be determined using e.g. cup method measurement, see [16]. Briefly, it is based on a continuous weighing of the sample mounted to cup exposed to a change in a relative humidity of surroundings. Considering the Fick's first law, it is possible to compute the diffusion coefficient from the measured weight loss over time. The measurement is further described in Section 5.6.

3.4 Thermal properties

Proper design of the energy efficient building can not be made without knowledge of thermal properties. Combustibility of the wood is well known for centuries, although this is an important property, it occurs only in extreme situation (during a fire) and is not a subject of this work. The same is for (calorimetric) heat value, which is defined as a quantity of heat that a mass unit of wood creates when it burns totally [5], important for the design of heating.

Most materials change their dimensions in relation to temperature, and wood is no exception. Dimensional expansion is characterized by the coefficient of thermal expansion, which is a measure of the relative change of dimension caused by temperature change [3]. In civil engineering, the linear thermal expansion coefficient $\alpha[K^{-1}]$ is mainly used. In both cases, the highest values is in the tangential direction and the lowest in the axial direction. Nevertheless, the dimensional changes with temperature are very small in comparison to that related to moisture [6].

The amount of heat required to raise the temperature of a unit mass [kg] by one degree [K] is a definition of specific heat or heat capacity c [J/kgK]. It is dependent on temperature and moisture content, whereas practically independent of density or species. The value for oven-dry wood is approximately 1360 J/kgK [4]. High value of the specific heat predetermines the wood as suitable for, e.g. handles. With a knowledge of the density, thermal conductivity and specific heat, it is possible to determine the thermal diffusivity describing how fast a material can absorb the heat from its surroundings (~0,0005 m^2/h) [5].

Among other thermal properties, the most attention will be devoted to thermal conductivity in this thesis. The thermal conductivity is a measure of quantity of heat [J] which will flow during a unit of time [s] through a material of unit surface area and thickness [m] when unit temperature difference [K] is maintained between two surfaces. It is expressed by coefficient of thermal conductivity $\lambda[W/mK]$or $\kappa[kcal/mh°C]$. The smaller the value is, the greater is the resistance of the material to the passage of heat. From that point of view the wood belongs to the poorest conductors. Thermal conductivity is influenced by many factors such as wood structure, density, moisture, temperature, extractives content, defects, microfibril angle etc. Above the fibre saturation point the conductivity is considerably higher than in the dry state. From that, the dry wood

is better thermal insulator. The values for spruce with density of 340 kg/m^3 are 0.10 W/mK in the transverse direction and 0.21 W/mK in the longitudinal direction [4].

Tab. 10 Thermal conductivities of individual wood constituents [10]

Phase	Material behaviour	$\lambda[W/mK]$
Hemicellulose	Isotropic	0.34
Lignin	Isotropic	0.39
Water + extractives	Isotropic	λ_{H_2O}
Lumen	Isotropic	λ_{air}
Cellulose	Transversely isotropic	$\lambda_{cell,11} = 0.26$
		$\lambda_{cell,22} = 0.26$
		$\lambda_{cell,33} = 1.04$

There are several techniques of the thermal conductivity measurement. They can be divided into two categories: steady-state methods and transient methods. The first one is based on a measuring the temperature difference at a distance under the steady-state heat flow. The thermal conductivity is therefore computed using Fourier's law. The absolute technique with a guarded-hot-plate apparatus as a typical test device, and comparative technique comprising comparative cut bar technique and heat flow meter method belong to the steady-state methods. The transient techniques include, e.g. pulsed power technique, hot-wire method and transient plane source (TPS) method (i.e. hot disk method) [17]. Or it could be determined employing empirical equations with density as the only variable. In [18] the author mentioned two equations for conditions with moisture content of 12%. The first one is in the form:

$$\kappa = 0.177\,\rho_{12} + 0.0205\,\left[\frac{kcal}{mh°C}\right] \tag{3.17}$$

where ρ_{12} [g/cm^3] is the air-dry density. And the second one is statistically derived by the author himself and reads:

$$\kappa = 0.168\,\rho_{12} + 0.022\,\left[\frac{kcal}{mh°C}\right] \tag{3.18}$$

where the air-dry density ρ_{12} [g/cm^3] is in the range of $0.2<\rho_{12}<0.8$.

More recent approach relies on the determination of wood thermal conductivity employing the homogenization techniques, see Chapter 6. For the computation, it is necessary to know thermal properties and volume fractions of individual wood constituents. According to [10], the thermal conductivities of individual wood constituents are summarized in Tab. 10. The thermal conductivity of lumens is set equal to the air thermal conductivity given as a function of temperature T [K]:

$$\lambda_{air} = 3.102\times10^{-4} + 9.5\times10^{-5}T - 2.917\times10^{-8}T^2 \tag{3.19}$$

where the influence of water vapour content is not considered. Because of low content of extractives, their impact on total thermal conductivity is neglected and therefore only the value of water is considered. The authors in [10] considered properties of the bound water as that of the free water. The thermal conductivity of the free water is given by:

$$\lambda_{H_2O} = -0.7282 + 7.299\times10^{-3}T - 9.454\times10^{-6}T^2 \tag{3.20}$$

where T is the actual temperature in [K].

4 Micromechanical homogenization

4.1 Theoretical background

The wood could be possibly described as the combination of the fibre reinforced composite and that of the cellular structure, made of natural based material. From that it belongs to the natural composites, as it was mentioned in the previous sections, and it will be treated as one of them.

Rapid development of composites over the last decades required a more precise determination of the behaviour of this material. The composites are generally heterogeneous materials, which requires the determination of many material constants and the computation of the behaviour becomes very difficult and time consuming. A suitable approach for simplification of the computational procedure could be the introduction of effective material properties, which reduces the number of constants. This could be accomplished by homogenization techniques. The homogenization provides an estimation of behaviour at a macroscale using information from a smaller length scales. From that it is necessary to know the structural composition of the composite and the material properties of individual constituents. The development of this method has also been contributed by the invention of the high-resolution microscopes with the help of which it is possible to study the microstructure of the material. Also, the measurement of the material properties at the microscale is possible nowadays, e.g. by nanoindentation.

Many authors have contributed to the theory of composites, micromechanics and homogenization. A short introduction to continuum micromechanics is provided by Böhm [19]. The micromechanical theory applied on composites is available in works by Milton [20] and Dvorak [21]. A practical application of micromechanics and composites is described by Šejnoha and Zeman [22]. It is also appropriate to mention the classical works that have become the basis of homogenization such as Eshelby [23], Hashin and Shtrikman [24], Mori and Tanaka [25], Hill [26] and many others.

Due to the similarity of the solutions, only the determination of the effective mechanical properties considering linear elasticity is described in the following. The governing equations in an elastic body at equilibrium and in the absence of the body forces take the form:

$$\boldsymbol{\sigma}(\boldsymbol{x}) = \mathbf{L}(\boldsymbol{x})\boldsymbol{\varepsilon}(\boldsymbol{x});\ \ \nabla \cdot \boldsymbol{\sigma}(\boldsymbol{x}) = 0;\ \ \boldsymbol{\varepsilon}(\boldsymbol{x}) = \frac{\left[\nabla u(\boldsymbol{x}) + \left(\nabla u(\boldsymbol{x})\right)^{T}\right]}{2} \tag{4.1}$$

where $\boldsymbol{\sigma}(\boldsymbol{x})$ is the stress field, $\boldsymbol{\varepsilon}(\boldsymbol{x})$ is the strain field that is symmetrized gradient of the displacement field $\mathbf{u}(\boldsymbol{x})$ and $\mathbf{L}(\boldsymbol{x})$ is the elasticity matrix. The constitutive relation could be written in an equivalent form:

$$\boldsymbol{\varepsilon}(\boldsymbol{x}) = \mathbf{M}(\boldsymbol{x})\boldsymbol{\sigma}(\boldsymbol{x}) \tag{4.2}$$

where $\mathbf{M} = \mathbf{L}^{-1}$is the compliance matrix [20]. The elasticity values are dependent on a position in a material. Endeavouring to determine effective elasticity matrix of the equivalent homogeneous material with overall behaviour, volume averages of the stress and strain fields are introduced as:

$$\langle\boldsymbol{\sigma}(\boldsymbol{x})\rangle = \mathbf{L}^{*}\langle\boldsymbol{\varepsilon}(\boldsymbol{x})\rangle;\ \ \langle\boldsymbol{\varepsilon}(\boldsymbol{x})\rangle = \mathbf{M}^{*}\langle\boldsymbol{\sigma}(\boldsymbol{x})\rangle \tag{4.3}$$

where $\mathbf{L}^{*}$ and $\mathbf{M}^{*}$are effective stiffness and compliance matrices, respectively. Local strain and stress fields of a given phase *r* and the overall macroscopic fields are linked together by strain and stress concentration factors $\mathbf{A}_r$ and $\mathbf{B}_r$ as follows:

$$\langle\boldsymbol{\varepsilon}_r\rangle = \mathbf{A}_r\langle\boldsymbol{\varepsilon}\rangle;\ \langle\boldsymbol{\sigma}_r\rangle = \mathbf{B}_r\langle\boldsymbol{\sigma}\rangle \tag{4.4}$$

Furthermore, the effective elastic matrices can be obtained from the local elastic matrices and concentration factors by volume averaging:

$$\begin{aligned} \mathbf{L}^{*} &= \frac{1}{\mathrm{V}}\int_{\mathrm{V}} \mathbf{L}(\boldsymbol{x})\mathbf{A}(\boldsymbol{x})\,\mathrm{dV}\,; \\ \mathbf{M}^{*} &= \frac{1}{\mathrm{V}}\int_{\mathrm{V}} \mathbf{M}(\boldsymbol{x})\mathbf{B}(\boldsymbol{x})\,\mathrm{dV} \end{aligned} \tag{4.5}$$

where V denotes the volume of a given representative element [19].

The majority of the modelling approaches may be divided into two groups. The first one comprises methods that describe interactions in a collective way in terms of phase-wise uniform fields, which are the mean-field approaches with related methods and bounding methods. In the second group, the approximations are based on studying discrete microgeometries in order to evaluate the microfields, and thereby take the

interactions between phases into account. It includes the periodic microfield approaches (often referred to as periodic homogenization schemes or unit cell methods), windowing approaches, embedded cell or embedding approaches and others.

Following the mean-field approach, the simplest case is the two-phase composite consisting of an elastic matrix strengthened by randomly dispersed spherical inclusions with perfect bonding between the constituents. To provide estimates of the effective properties we assume that the composite is subjected to boundary displacements compatible with macroscopically uniform strains or tractions compatible with macroscopically uniform stresses. An average stress in the composite could be written as:

$$\langle \boldsymbol{\sigma} \rangle = f_1 \langle \boldsymbol{\sigma}_1 \rangle + f_2 \langle \boldsymbol{\sigma}_2 \rangle \tag{4.6}$$

where f_r denotes the volume fraction of phases r, where $\sum_r f_r = 1$. Equivalently an average strain is given as:

$$\langle \boldsymbol{\varepsilon} \rangle = f_1 \langle \boldsymbol{\varepsilon}_1 \rangle + f_2 \langle \boldsymbol{\varepsilon}_2 \rangle \tag{4.7}$$

Combination of Eqns. (4.6) and (4.7) together with assumption of the constant stiffness matrix $\mathbf{L}_r$ within the phase r yields to [27]:

$$\langle \boldsymbol{\sigma} \rangle = \mathbf{L}_1 \langle \boldsymbol{\varepsilon} \rangle + f_2 (\mathbf{L}_2 - \mathbf{L}_1) \langle \boldsymbol{\varepsilon}_2 \rangle \tag{4.8}$$

A unique dependence of the average strains in the phases upon the overall strain in the composite is written as [26]:

$$\langle \boldsymbol{\varepsilon}_1 \rangle = \mathbf{A}_1 \langle \boldsymbol{\varepsilon} \rangle;\ \langle \boldsymbol{\varepsilon}_2 \rangle = \mathbf{A}_2 \langle \boldsymbol{\varepsilon} \rangle;\ f_1 \mathbf{A}_1 + f_2 \mathbf{A}_2 = \mathbf{I} \tag{4.9}$$

where $\mathbf{I}$ is the identity matrix. Using (4.3) and (4.9) Eq. (4.8) can be transformed to:

$$\mathbf{L}^* = \mathbf{L}_1 + f_2 (\mathbf{L}_2 - \mathbf{L}_1) \mathbf{A}_2 \tag{4.10}$$

Equivalently the effective compliance of the composite is given by:

$$\mathbf{M}^* = \mathbf{M}_1 + f_2 (\mathbf{M}_2 - \mathbf{M}_1) \mathbf{B}_2 \tag{4.11}$$

Assuming that the strain throughout the composite is uniform and therefore the strain concentration factors $\mathbf{A}_1 = \mathbf{A}_2 = \mathbf{I}$, it yields the Voigt approximation written as:

$$\mathbf{L}^*_{Voigt} = \mathbf{L}_1 + f_2(\mathbf{L}_2 - \mathbf{L}_1) = f_1\mathbf{L}_1 + f_2\mathbf{L}_2 \tag{4.12}$$

which provides the estimate of the upper bound of the effective properties. Whereas the lower bound was developed by Reuss with the assumption that the composite experiences the same stress in every phase identical to the one in an equivalent homogeneous material. Thus the stress concentration factors $\mathbf{B}_1 = \mathbf{B}_2 = \mathbf{I}$. The effective stiffness is therefore:

$$\mathbf{L}^*_{Reuss} = [\mathbf{M}_1 + f_2(\mathbf{M}_2 - \mathbf{M}_1)\mathbf{B}_2]^{-1} = [f_1\mathbf{L}_1^{-1} + f_2\mathbf{L}_2^{-1}]^{-1} \tag{4.13}$$

In case of lamination theory used in the following sections the Voigt approximation corresponds to the parallel connection of lamellae and the Reuss approximation to the connection in series. The prediction of the effective moduli of the composite is performed by the Self-consistent and Mori-Tanaka methods. The two methods will be described separately in individual sections.

4.2 Classical Self-consistent scheme

The Self-consistent method belongs to the effective medium approaches. The method is based on treating all phases as inhomogeneities, where each subvolume of phase $\mathbf{L}_r$ is embedded as a solitary ellipsoidal inclusion in a large volume of an a priori unknown effective medium. An overall stress or strain is applied at the remote boundary. The concentration factors of each phase are therefore [21]:

$$\begin{aligned} \mathbf{A}_r^{SC} &= [\mathbf{I} + \mathbf{P}(\mathbf{L}_r - \mathbf{L}_{SC})]^{-1} \\ \mathbf{B}_r^{SC} &= [\mathbf{I} + \mathbf{Q}(\mathbf{M}_r - \mathbf{M}_{SC})]^{-1} \end{aligned} \tag{4.14}$$

where **P** is the so called Hill tensor and is linked by relation:

$$\mathbf{P} = \mathbf{S}\mathbf{M}_0 = \mathbf{S}\mathbf{L}_0^{-1}\ ;\ \mathbf{PL}+\mathbf{MQ}=\mathbf{I} \tag{4.15}$$

to the Eshelby tensor **S**, where $\mathbf{M}_0$ and $\mathbf{L}_0$ are the host medium compliance and stiffness matrices, respectively, which in the case of Self-consistent scheme are $\mathbf{M}_0 = \mathbf{M}_{SC}$ and $\mathbf{L}_0 = \mathbf{L}_{SC}$. Recall that in the case of Self-consistent method the Eshelby and Hill tensors elaborated in [28] are also functions of the properties of the host medium. Generalizing the relationships for effective stiffness and compliance of the two-phase composite to the multi-phase one, it is possible to rewrite (4.10) and (4.11) as:

$$\mathbf{L}_{SC}^{*} = \mathbf{L}_1 + \sum_{r=2}^{N} f_r(\mathbf{L}_r - \mathbf{L}_1)\mathbf{A}_r^{SC}$$
$$\mathbf{M}_{SC}^{*} = \mathbf{M}_1 + \sum_{r=2}^{N} f_r(\mathbf{M}_r - \mathbf{M}_1)\mathbf{B}_r^{SC} \tag{4.16}$$

This method is well suitable for systems where the role of matrix and inclusion could be reversed. However, it could not be employed for porous materials. Point out finally that the effective properties occur on both sides of the relationship (4.16) and it leads to the iterative solution [22].

4.3 Mori-Tanaka method

The Mori-Tanaka method pertains to the mean-field estimates. In contrary to the previously mentioned method, the Mori-Tanaka method has an explicit format. The method approximates the interaction between the phases in a matrix-based system by considering each inhomogeneity $\mathbf{L}_r$ as a solitary inclusion embedded in an unbounded matrix $\mathbf{L}_1$. The interaction of inclusions is accomplished by loading the system by an average stress or strain found in the matrix. The determination of effective material properties is similar to the one in the previous section employing the pertinent concentration factors. For a two-phase composite they are provided by:

$$\mathbf{A}_2^{MT} = \mathbf{A}_2^{dil}\left[f_1\mathbf{I} + f_2\mathbf{A}_2^{dil}\right]^{-1};\ \mathbf{A}_2^{dil} = [\mathbf{I} + \mathbf{P}(\mathbf{L}_2 - \mathbf{L}_1)]^{-1}$$
$$\mathbf{B}_2^{MT} = \mathbf{B}_2^{dil}\left[f_1\mathbf{I} + f_2\mathbf{B}_2^{dil}\right]^{-1};\ \mathbf{B}_2^{dil} = [\mathbf{I} + \mathbf{Q}(\mathbf{M}_2 - \mathbf{M}_1)]^{-1} \tag{4.17}$$

where for individual members, the same relationships apply as in the previous section. Note that in this case the **P** and **Q** terms depend on the matrix properties. Finally, estimates of the effective stiffness and compliance matrices of the multi-phase composite can be obtained from:

$$\mathbf{L}_{MT}^{*} = \mathbf{L}_1 + \left[\sum_{r=2}^{N} f_r(\mathbf{L}_r - \mathbf{L}_1)\mathbf{A}_r^{dil}\right]\left[f_1\mathbf{I} + \sum_{r=2}^{N} f_r\mathbf{A}_r^{dil}\right]^{-1}$$
$$\mathbf{M}_{MT}^{*} = \mathbf{M}_1 + \left[\sum_{r=2}^{N} f_r(\mathbf{M}_r - \mathbf{M}_1)\mathbf{B}_r^{dil}\right]\left[f_1\mathbf{I} + \sum_{r=2}^{N} f_r\mathbf{B}_r^{dil}\right]^{-1} \tag{4.18}$$

where $\mathbf{A}_r^{dil}$ and $\mathbf{B}_r^{dil}$ are given by Eqns. in (4.17) and satisfy the relationship $\mathbf{I} = \sum_{r=1}^{N} f_r \mathbf{A}_r^{dil}$ and $\mathbf{I} = \sum_{r=1}^{N} f_r \mathbf{B}_r^{dil}$, respectively [22].

In composites with large contrast between moduli of the constituents, the Mori-Tanaka tends to underestimate (or overestimate) effective moduli, even at moderate concentrations. In case of porous two-phase media it leads to the upper Hashin-Shtrikman bound, which approaches zero only when the matrix volume fraction reaches zero [21].

5 Experimental determination of wood properties

Some of the properties mentioned in Chapter 3 were measured on small clear samples of the Norway spruce (*Picea abies*). Factors affecting the properties, such as knots, grain deviations, resin streaks, bark pockets etc., were kept to a minimum. Tensile tests were performed on 40 samples, of which 19 were used for the density and moisture content measurement, together with image analysis of the growth rings, and 6 of them were measured by nanoindentation and examined by microscopy. Another 27 samples were used for the density and moisture content determination and image analysis of the growth rings.

5.1 Density and moisture content

Small samples of clear wood were cut from the dog bone specimens made from Norway spruce. They were conditioned for few days at room temperature and relative humidity, which corresponds to the air-dry state. The dimensions of all samples were measured to the nearest 0.01 mm by digital caliper at both ends in each of the three directions. Then the measured values were averaged and the volume of each sample was computed. Initial masses of air dried wood specimens were obtained using laboratory scales with an accuracy of 0.01 μg. After that, the samples were put into an oven and left there at a temperature of 40°C. All of them were periodically weighed until the differences between the two consecutive measurements were negligible. In about seven days there were no weight losses and the measurement was terminated.

Tab. 11 Measured values of the moisture content and densities

		mean	min	max
Air-dry density	$[kg/m^3]$	441.80	380.33	527.58
Oven-dry density	$[kg/m^3]$	422.73	365.34	510.23
Moisture content	[%]	4.50%	3.40%	5.17%

Resulting values of air-dry density and oven-dry density were computed from Eq. (3.1), where in the first case *m* was set equal to the initial mass, whereas in the latter one the mass corresponds to that measured as the last – oven-dry mass. The gravimetric moisture content was calculated by Eq. (3.8). The measurement was made on 45 samples in total and its mean, minimum and maximum values are summarized in Tab. 11.

The average value of the oven-dry density is 422.73 kg/m^3, that of the air-dry density is 441.80 kg/m^3 and the resulting average gravimetric moisture content is 4.5%. Example values of the moisture content and densities for 5 samples are mentioned in Tab. 3, which are subsequently used for the computation of the volume fractions. The measured initial and oven-dry masses with corresponding moisture content are summarized in Tab. 9 for five samples as an example.

5.2 Volume fractions of the earlywood and latewood

The knowledge of the volume fractions of the earlywood and latewood is important for the last step of the homogenization procedure. The samples prepared for the previous measurement, i.e. density and MC measurement, were used. Surfaces localized on cross sections were ground to obtain sufficient contrast between phases. Afterwards, pictures of the surfaces were taken with common photo camera.

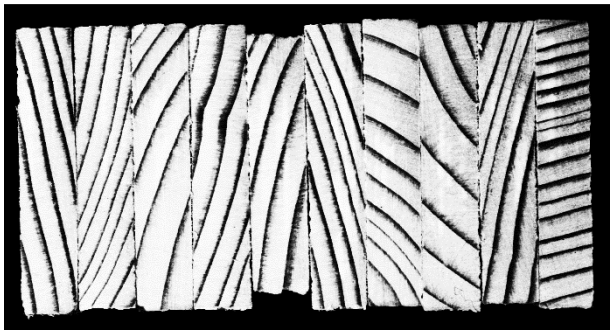

Fig. 9 Cross sections of the spruce samples

Subsequent editing of photographs by commercial software increased the contrast of the borders between individual phases (Fig. 9) and the image analysis could be performed. Recalling Fig. 9, it shows a great variability of the growth rings arrangement. Several parameters were measured: growth ring width, width of the latewood part, volume fractions of black (latewood) and light (earlywood) parts related to total area of one sample. The volume fractions of the earlywood and latewood parts were obtained by two approaches. The first one was the direct determination from photographs by image analysis and in the second one the volume fractions were calculated from measured widths. Mean, minimum and maximum values of these parameters are summarized in Tab. 12. As it is evident from Tab. 12, the volume fractions of earlywood computed from widths are higher than those obtained by image analysis. It could be attributed to the fact that the image analysis involves the distribution of individual phases throughout the

sample. Whereas the width of one growth ring was measured at the selected location and from that it does not include the change over the length of the growth ring.

Tab. 12 Measured parameters of growth rings

	mean	min	max
Growth ring width [*mm*]	1.73	0.60	3.40
Latewood width [*mm*]	0.23	0.06	0.61
Volume fractions (IA) [-]			
Earlywood	0.80	0.69	0.94
Latewood	0.20	0.06	0.31
Volume fractions (widths) [-]			
Earlywood	0.86	0.77	0.94
Latewood	0.14	0.06	0.23

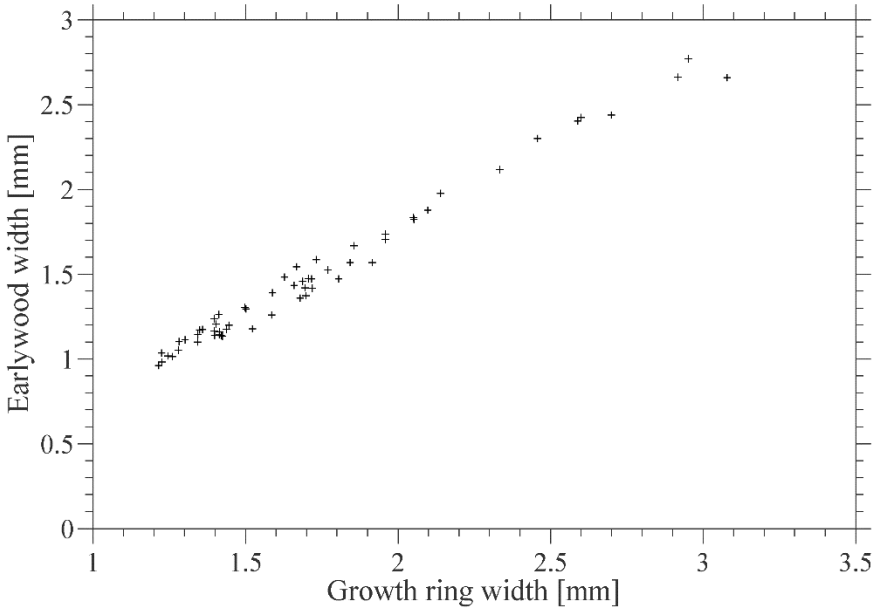

Fig. 10 Dependence of the earlywood width on the growth ring width

During the measurements, the dependence of the earlywood width on the overall width of the growth ring was found, see Fig. 10, where the linear correlation between both parameters is obvious. On the other hand, no correlation was found between latewood width and growth ring width, see Fig. 11. With regard to both phenomena, it is possible to consider the latewood width as constant (set to 0.2 mm in the following) and

earlywood width as the only one variable. Similar conclusion has been put forward by [13].

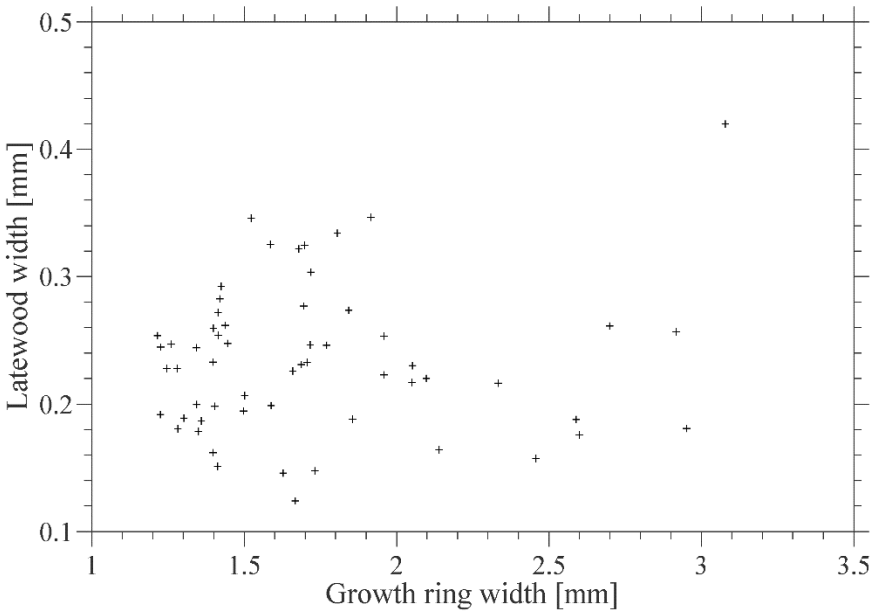

Fig. 11 Dependence of the latewood width on the growth ring width

When we plot the dependence of the earlywood width on the oven-dry density, the correlation between these values is evident, see Fig. 12. The same correlation also applies to the dependence of the earlywood volume fraction on oven-dry density, assuming constant latewood width and computation of the volume fractions using measured widths. This ascertainment allows us to adopt an assumption that the density of wood is dependent on the volume fraction of earlywood, where higher fraction of earlywood results in lower density. If we find a suitable function which will fit the data well, the volume fractions of the earlywood and latewood could be computed reversibly for known density.

Recalling the computation of the volume fractions described in Section 3.1, Eqns. (3.6) are linear functions, while the dependence depicted on Fig. 12 seems to be rather exponential. When the volume fractions computed from the measured widths assuming constant latewood width (0.2 mm) and Eqns. (3.6) are plotted in one figure (Fig. 13), it is evident that the measured data are rather outside the lines representing equations stated by the authors in [10]. Plus signs in the upper part of the image represent the volume fractions of earlywood and that in the lower part represent the latewood volume fractions. The picture also shows that the volume fractions computed by Eqns. (3.6) are equal if the density is 472 kg/m^3. When the density approaches the value of 600 kg/m^3, the volume

fraction of earlywood is reaching zero and the latewood volume fraction is close to 1. It means that wood with density close to 600 kg/m^3 is almost composed of pure latewood, which is not a reasonable assumption. The same applies to the other bound of the interval, but inversely. In [13] the author stated that the density of clear wood specimens of Norway spruce is about 350-600 kg/m^3. According to the graphs published in this work, even the values outside the interval were measured, which makes these equations inapplicable. This leads to the decision about inaccuracy of these equations.

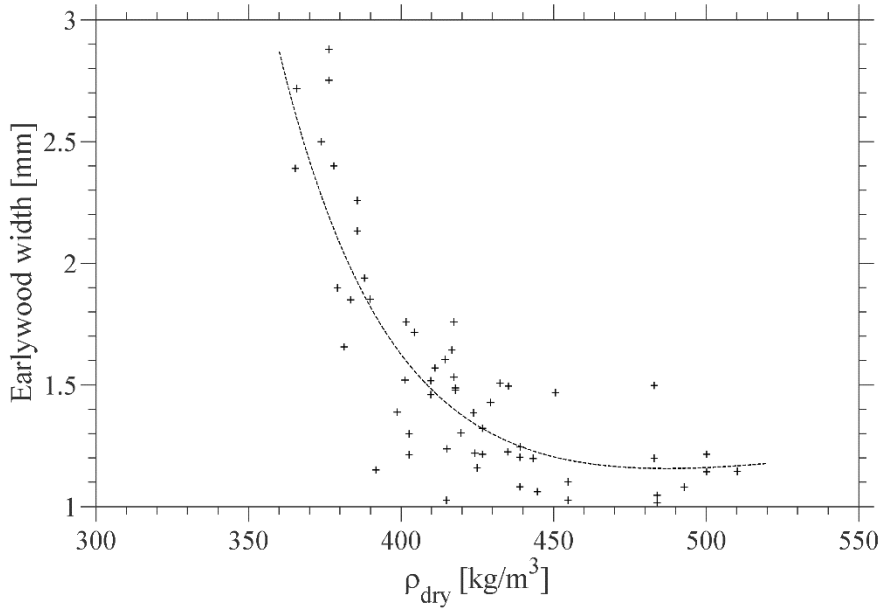

Fig. 12 Dependence of the earlywood width on the oven-dry density (with illustrative fit function)

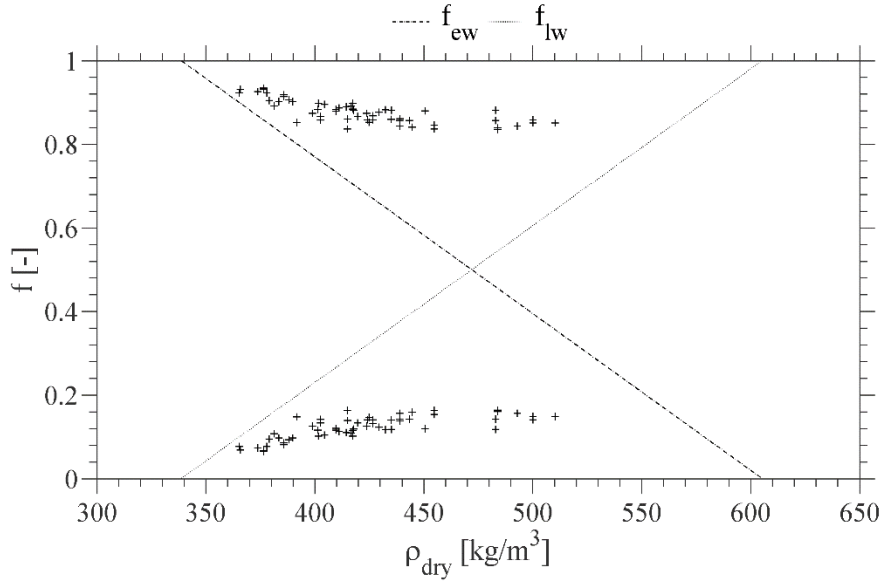

Fig. 13 Dependence of the earlywood and latewood volume fractions on oven-dry density

5.3 Volume fractions of pores

Accurate determination of the volume fractions of lumens is a key factor for the homogenization procedure. Pores are assumed to decrease the final effective properties. Incorrect values of the lumen volume fractions lead to great errors in the results. However, the determination of the size and distribution of pores within the wood sample is still a great challenge. Many approaches exist nowadays, e.g. porosimetry, CT scans etc. and each of them has its advantages and disadvantages. Some of them have been already mentioned in Section 3.1 and compared in Tab. 4. This section is mainly focused on the determination of the lumens volume fractions using the image analysis.

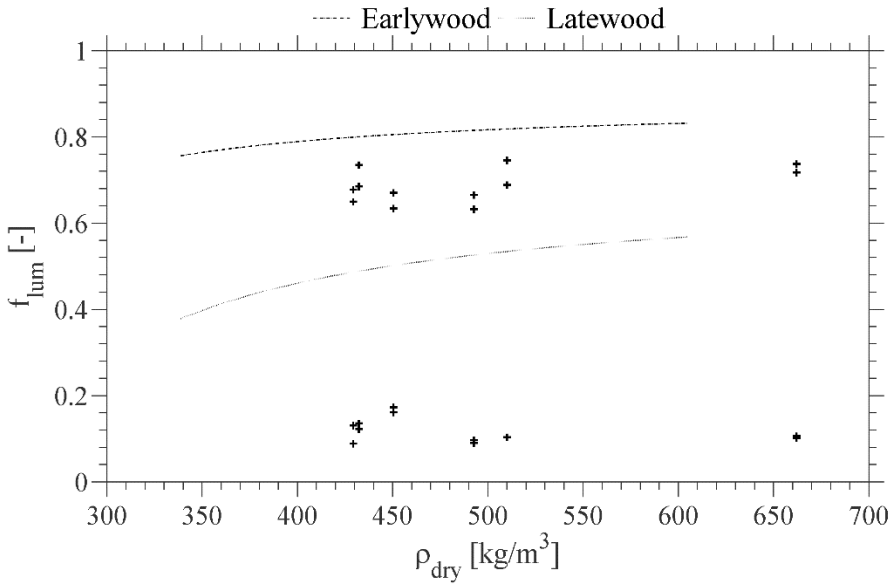

Fig. 14 Dependence of the volume fractions of lumens on oven-dry density

The sample preparation is similar to that in the case of nanoindentation, see Section 5.5. Small clear samples of the Norway spruce were embedded in an epoxy resin. After the resin hardened enough, the samples were cut into slices with diamond wheel at small revs. The cuts were performed perpendicularly to the longitudinal direction. One side of each slice was ground and polished to obtain as smooth surface as possible. This step is necessary to prevent the defibrillation of the structure, which leads to lower visibility of the cell wall edges. Afterwards, the specimens were examined by microscope with simultaneous image capturing. The images were subsequently edited by commercial software and transformed to binary images, where white colour corresponds to lumens and black to the cell wall material, see Fig. 6 as an example. The main task of the image

analysis is to determine the size of black and white areas in relation to the whole image. The earlywood and latewood cells were examined separately, whereas that of the transition wood were excluded from the analysis, i.e. influence of the transition zone was neglected. As it was proposed in Section 3.1, the volume fractions of lumens for both the earlywood and latewood can be computed combining Eqns. (3.3), (3.4) and (3.5). Both results from the image analysis and equations represented by curves are depicted on Fig. 14, where the plus signs in the upper part are the volume fractions of earlywood lumens and that in the lower part represents the volume fractions of latewood lumens. The data from image analysis are rather constant, i.e. they do not show any dependence on the density, even in the case of a very high density (points on the right-hand side). Therefore, the average values of 0.69 for the earlywood and 0.12 for the latewood are considered in the homogenization procedure. From Fig. 14 it is evident that the values derived by Eqns. (3.3),(3.4) and (3.5) are overestimated, especially in the case of the latewood lumens (lower curve). It is reasonable to cast doubt on the computational approach, which was already proposed in Section 3.1.

5.4 Tensile tests

One of the possible ways of determining the modulus of elasticity is the axial tensile test. The samples with a shape of ‘dog bone’, i.e. long thin veneers with widening on both ends, were cut from Norway spruce timber, see Fig. 15. This shape enables the fraction to occur in the middle instead of the zone of grip.

Fig. 15 Dog bone sample for the axial tensile test

Samples were tested one at a time. Each sample was fastened into grips of the testing machine and extensometer with length of 100 mm was placed to the middle part of the specimen. Afterward, the sample was loaded in tension in a displacement control regime until failure, with simultaneous recording of the load and elongation of the extensometer. The modulus of elasticity is defined as an initial slope of the stress-strain curve. The stress is computed as the applied force divided by the area of the cross section in the middle of the sample and the strain is given as the extensometer expansion divided by its initial length. The resulting values are plotted in the form of normal distribution, see Fig. 16. The mean value is 14.29 MPa and thus lies within a range given in Tab. 5.

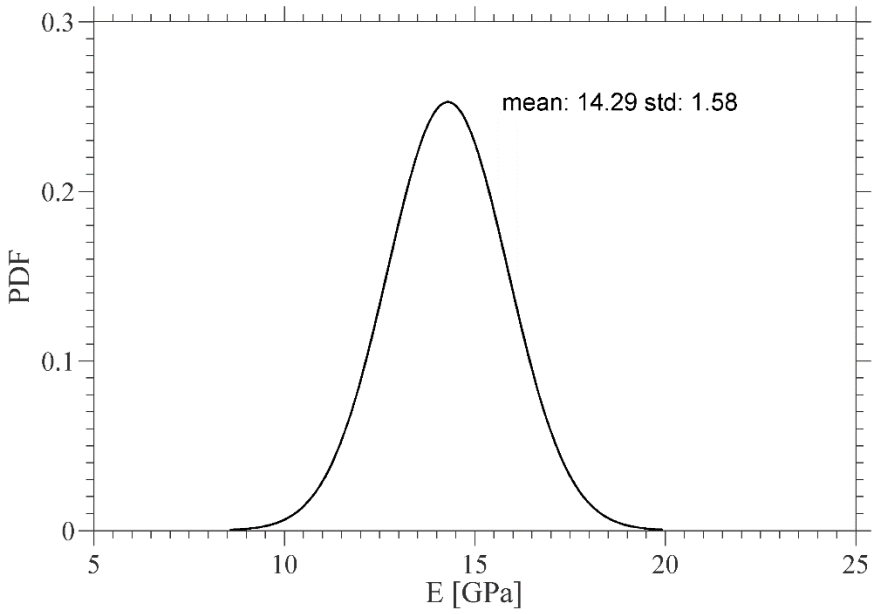

Fig. 16 Probability density function of modulus of elasticity from axial tensile test

5.5 Nanoindentation

The mechanical properties of the cell wall could be measured directly by nanoindentation. The nanoindentation is used for the characterization of mechanical behaviour of materials at the micrometre and nanometre scales. This method is based on the contact mechanics with limitations for some types of material responses e.g. viscoelastic solids. The method was developed for measuring hardness and elastic modulus from load-displacement data, obtained during one cycle of loading and unloading by using sharp, self-similar indenters, such as the Berkovich triangular pyramid. The basic principle of this method is pushing the small hard tip with known geometry and material properties to a material with unknown properties, with simultaneous recording of the load and indentation depth relative to the initial undeformed surface. The load-displacement curve is depicted on Fig. 17, where P_{max} is the maximum load, h_{max} is the maximum displacement, $S=dP/dh$ is the elastic unloading stiffness defined as the slope of the upper part of the unloading curve and h_f is the final depth – the permanent penetration depth after the indenter is fully unloaded. In this model, the elastic and plastic deformation during loading is assumed, whereas during unloading only elastic displacements are recovered [29]. The maximum force holding is used to eliminate the viscoelastic response of the material, which is very important in the case of wood, because it exhibits viscoelasticity.

Probably, the most used tip is the Berkovich indenter (also used in this thesis), which can be modelled by a conical indenter with a half-included angle ϕ = 70.3°, that gives the same depth-to-area relationship. Very important is the assumption that the contact periphery sinks in in compliance with the models of indentation of a flat elastic half-space by rigid punches of simple geometry [29].

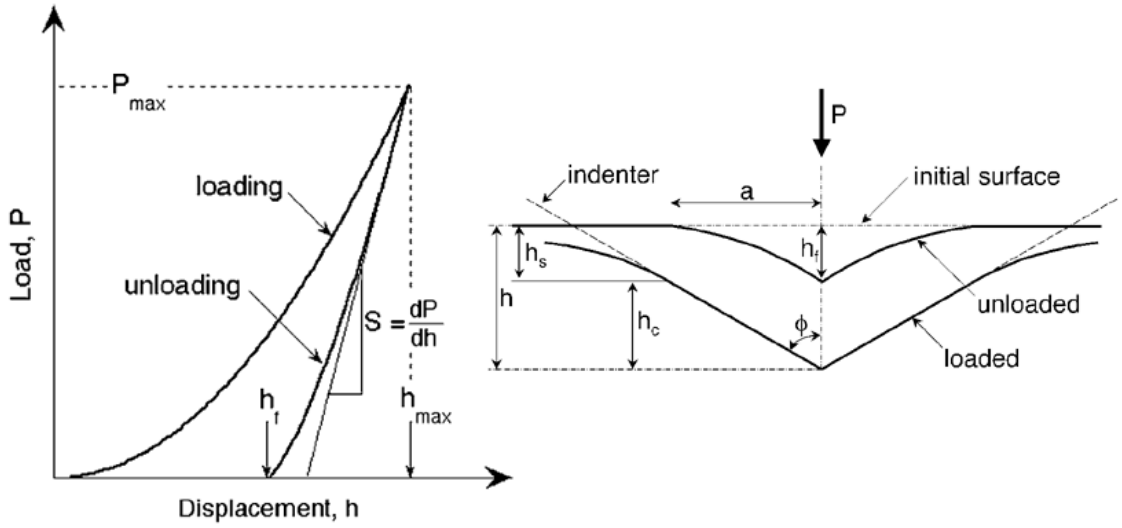

Fig. 17 Load-displacement curve and unloading process of the indenter tip [29]

The main output of the nanoindentation is the indentation modulus. The indentation modulus E_r (also called reduced modulus) is quantified from the measured data as follows [29]:

$$E_r = \frac{\sqrt{\pi}}{2\beta}\frac{S}{\sqrt{A}} \tag{5.1}$$

where $S=dP/dh$ is the slope od the unloading part of the load-displacement curve (the elastic unloading stiffness), a is the contact area and the correction factor β, which is the dimensionless parameter of the indenter tip geometry. Probably, the most accurate would be the direct measurement of the contact area of each indent, however it is not possible nowadays. The size of the residual impression of the indenter is too small to be measured accurately. From that the area function was introduced. In the case of Hysitron nanomechanical test instrument, which is used for the measurement in this thesis, the area function is given by a sixth order polynomial of the form [30]:

$$A = C_0 h_c^2 + C_1 h_c + C_2 h_c^{1/2} + C_3 h_c^{1/4} + C_4 h_c^{1/8} + C_5 h_c^{1/16} \tag{5.2}$$

where h_c is the contact depth and $C_0 - C_5$ are the calibration constants obtained by a calibration process. The calibration is usually performed as an independent measurement on a material with known properties, e.g. fused silica. This procedure eliminates the influence of the deviations from an ideal tip geometry, such as rounding of the tip. As a result, the calibration should be made for each indenter individually. However, this area function does not account for a pile-up of the material around the perimeter of the contact area. If there is the pile-up, the contact area is greater than the computed one and therefore the modulus is overestimated. When the ratio of the final indentation depth h_f to the maximum displacement h_{max} is over the value 0.7, using this method can lead to large errors in the contact area [29].

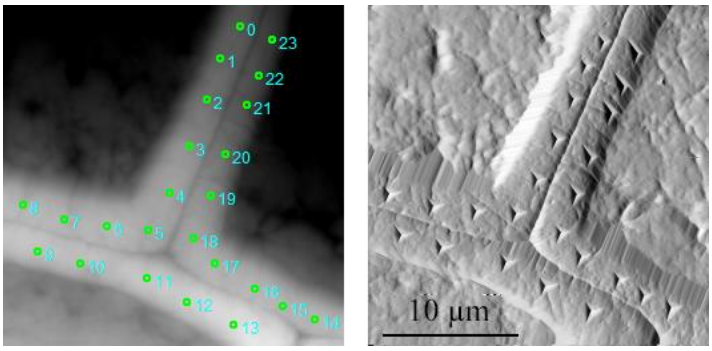

Fig. 18 Surface scan (25x25 µm) of earlywood before (left) and after (right) nanoindentation

The measurement was performed on small samples of the Norway spruce prepared by following procedure. Small enough samples were cut from the timber and left in a room to accommodate to the temperature and relative humidity of the surroundings. Then all cut samples were fixed in small containers and the epoxy resin was poured over them. For the elimination of unwanted gas, it was necessary to place samples into the vacuum desiccator and left there at low vacuum for a while. The epoxy fills in the lumens, but the question is, if it pours into the cell wall and affects the measurement results. Next, the embedded samples were cured at room temperature until they hardened enough. It is much better to avoid the heat treatment, which is usually used for the epoxy hardening, because the exposure to heat may affect the properties and the results of the measurement can exhibit inaccuracies. Then the cured samples were cut into slices with diamond cut-off wheel at low revs. One side of each slice was therefore ground and polished to obtain as smooth surface as possible. The surface roughness plays a significant role, because it affects the results, when it is too large.

It is very important to set-up the measurement device and to choose a proper type of the indentation tip. The Berkovich diamond indenter tip was used for measurement in this thesis. Although the author in [31] recommends small acuity spherical probes (e.g. A cono-spherical probe) also suitable for indentation of polymers, which exhibit viscoelastic response. Important settings are the load-time curve and the maximum depth. The load-time curve was set as a trapezoidal function containing three parts: linear loading, holding at peak load and linear unloading. The holding part is implemented to allow the plastic deformation to be fully realised in the case of materials, where the creep occurs. The indentation depth should be set higher than the measured surface roughness. After successful setting of the device, the measurement can be performed.

The samples should be accommodated to the temperature and humidity inside the chamber of the measurement device. The indents were localized into the S_2 layer using an added microscope. This layer was chosen with regard to its greatest impact on overall mechanical properties, as mentioned in Section 2.3. The positions of the indents should be controlled after the measurement with the help of surface scans, see Fig. 18. Indents on the wrong position have to be excluded from further data evaluation, together with those with the wrong shape of the load-displacement curve.

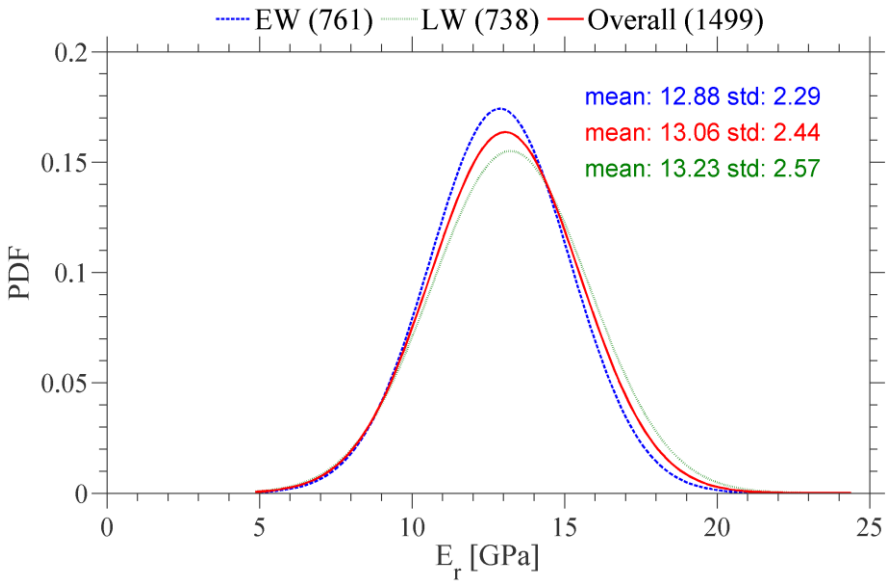

Fig. 19 Probability density function of indentation modulus

Considering the normal distribution, resulting mean values of earlywood (EW) and latewood (LW) are 12.88 GPa and 13.23 GPa, respectively. Because these values are very similar, it is possible to consider that the properties of the cell wall are the same

throughout the whole growth ring. Individual distributions are depicted on Fig. 19, where the similarity is more evident. The numbers in brackets correspond to the number of indents.

5.6 Measurement of the moisture diffusion coefficient

The last measured quantity was the moisture diffusion coefficient. The measurement was performed at the Department of materials, Faculty of Civil Engineering, CTU in Prague. The wet cup arrangement of the cup method was used considering steady-state under isothermal conditions. Samples of the Norway spruce with square cross section of 100x100 mm and thicknesses of 4, 6, 8 and 10 mm were fastened on the top of a cup and insulated with epoxy resin on edges to ensure one-dimensional water vapour transport. Each cup contained saturated solution of KNO_3 with equilibrium humidity of 95±5% above it. A thin layer of air (10 mm) was left between the solution and sample. The cups were placed into the climate chamber with controlled temperature and relative humidity. The step change of the relative humidity from 95% to 50% was carried out at temperature of 23°C. The cups were weighed periodically until the mass loss per time unit was constant. The resulting water vapour diffusion coefficients D [m^2/s] were computed from measured data as follows [32]:

$$D = \frac{\Delta m\ t\ R\ T}{A\ \tau\ M\ \Delta p} \tag{5.3}$$

where Δm [kg] is the amount of the water vapour diffused through the sample, t [m] the sample thickness, R = 8.314472 [$J/mol.K$] the universal gas constant, T [K] the actual temperature, a [m^2] the area of the specimen surface, τ [s] the duration of the transport of water vapour mass Δm, M = 0.018 [kg/mol] the molar mass of water, Δp [Pa] the difference in partial water vapour pressures above and under the specific specimen surface. The computed diffusion coefficients for various thicknesses are listed in Tab. 13.

Unfortunately, measured values are quite far from those given in the literature. For example, in [33] the author states that the typical value of the longitudinal diffusivity coefficient of Swedish pine and spruce is 1.5×10^{-9} m^2/s, determined at RH=75% considering steady-state. Therefore, these values were not considered for the verification of results obtained by the homogenization procedure.

Tab. 13 Moisture diffusion coefficients of spruce wood for various thicknesses

t [mm]	D [m^2/s]
4	4.90×10^{-6}
6	4.83×10^{-6}
8	5.50×10^{-6}
10	5.18×10^{-6}

6 Application of homogenization to wood

As it was mentioned earlier the wood is a natural composite and could be treated as such. In spite of the variability at all scales it is possible to consider it more or less as regular on average. Recalling the structural composition described in Chapter 2 the most appropriate approach to the determination of effective properties seems to be an upscale homogenization, which comprises several steps starting from the lowest scale up to the macroscale. An example of hierarchical organization of the wood is depicted on Fig. 20 at three different magnifications.

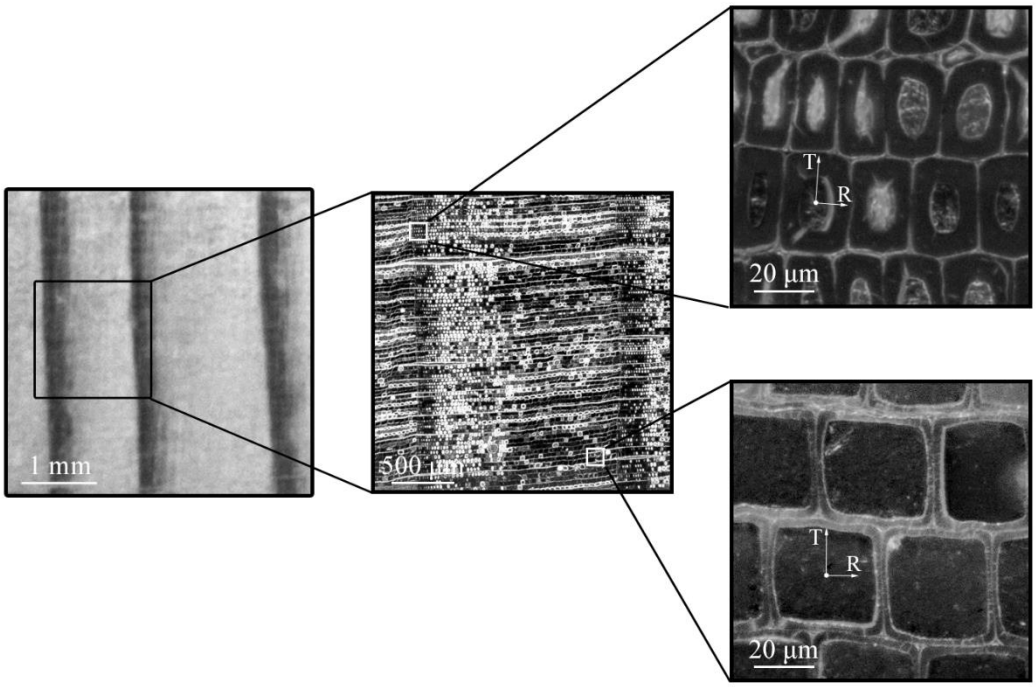

Fig. 20 Hierarchical organization of wood

It is possible to begin at the level of atoms, but it is too much complicated and the wood composition is not even known at the atomic level. A reasonable starting point of the micromechanical homogenization seems to be at the level of cell wall constituents. Following the homogenization procedure described in [9], the first step is called the polymer network with characteristic length of a representative volume element (RVE) in a range of 8-20 nm. The polymer network comprises lignin, hemicellulose, water and extractives, where the latter two phases are considered as one, because of the dissolution of the extractives in the water. Consequently, the relationship of the volume fractions of phases is given by:

$$\hat{f}_{lig} + \hat{f}_{hemcell} + \hat{f}_{we} = 1 \tag{6.1}$$

The volume fractions of all cell wall constituents are dependent on the moisture content and could be computed by equations introduced in [9] as:

$$f_s = WF_s^{wet} \frac{\rho_{cw}^{wet}}{\rho_s};\ WF_s^{wet} = \frac{WF_s^{dry}}{1+u} \tag{6.2}$$

where ρ_{cw}^{wet} is the density of the wet cell wall given by Eq. (3.4), WF_s^{dry} and ρ_s are weight fraction and density of each cell wall constituent (values were taken from [9]) and u is the moisture content of the cell wall. It is necessary to note that the volume fractions of the polymer network phases computed by (6.2) are determined relative to the entire cell wall and thus they have to be recalculated in relation to the polymer network, i.e. the volume fraction of the polymer network is:

$$f_{lig} + f_{hemcell} + f_{we} = f_{PN} \tag{6.3}$$

and therefore the volume fraction of phases in (6.1) are given by:

$$\hat{f}_s = f_s / f_{PN} \tag{6.4}$$

where $s \in$ {lignin, hemicellulose, water + extractives}. Lignin and hemicellulose are almost of the same volume fractions and the role of matrix and inclusion is not clear. From that a suitable method for this computational step seems to be the Self-consistent scheme with spherical inclusions in an isotropic matrix.

Effective properties of the cell wall material are obtained via the second step, where the characteristic length of RVE falls within a range of 0.5-1 μm. Remaining cell wall constituents that were not taken into account earlier are the amorphous and crystalline cellulose. These are in the form of long threads wound helically along the cell, see Section 2.3. It leads to the notion of these phases as infinite cylindrical inclusions. The polymer network determined by the previous step is set as a matrix and the volume fractions of phases are computed using Eqns. (6.2) and (6.3) and the relation takes the form:

$$f_{PN} + f_{crycell} + f_{amocell} = 1 \tag{6.5}$$

In this step influence of the microfibril angle is implemented as a deviation of inclusions from the longitudinal direction (axis x_3 in this thesis). Assumption of this structural composition leads to the Mori-Tanaka method for isotropic matrix with infinite circular cylindrical inclusions, which are deviated by an angle corresponding to MFA. Within this step the orientation averaging is implemented to obtain transversely isotropic material.

Following the wood composition, the next step covers the influence of the porous structure. Recalling Section 2.2, pores are in the form of ellipsoidal cavities – lumens, that change their shape within a single growth ring. For simplicity only division to earlywood and latewood is considered, while the transition zone (gradual change between both types) is neglected. The homogenization model is made up of the cell wall forming the matrix and lumens as ellipsoidal inclusions parallel to the longitudinal axis of the cell wall, assuming that:

$$f_{cw} + f_{lum} = 1 \tag{6.6}$$

where f_{cw} and f_{lum} are the volume fraction of the cell wall material and lumens, respectively. It is important to note that the volume fraction and shape of lumens differ for both the earlywood and latewood. The volume fractions of lumens could be computed using dry wood density or measured directly, referring to Section 3.1. The dimensions of lumens could be measured directly, e.g. by microscopy, or computed using the procedure described in [10]. The measured values of the cell dimensions for both earlywood and latewood were taken from the literature [5], see also Tab. 1, where after subtraction of the cell wall thickness the lumen dimensions are obtained, see Tab. 14.

Tab. 14 Dimensions of lumens [μm] [5]

	Radial	Tangential	Longitudinal
Earlywood	36.3	29.7	2657.0
Latewood	3.1	22.1	2650.0

The Mori-Tanaka method with ellipsoidal inclusions in transversely isotropic matrix was employed for the computation of the effective properties. Mainly because, unlike the Self-consistent scheme, this method is well suitable for materials with a porous phase. The resulting effective material is orthotropic, which correspond to the assumption of wood behaviour.

The last step utilizes the similarity of the growth ring arrangement with multi-layered laminate. Earlywood and latewood are aligned in plies, which leads to the application of standard rules of mixture. The Voigt and Reuss bounds are obtained employing Eqns. (4.12) and (4.13), where the volume fractions could be computed or measured, see Section 3.1, satisfying the condition:

$$f_{ew} + f_{lw} = 1 \tag{6.7}$$

where f_{ew} and f_{lw} are the volume fractions of earlywood and latewood, respectively. Recalling the growth ring arrangement and the definition of directions (Section 2.1) the selection of the type of the bound is dependent on the direction. Lamellae in the radial direction resembles the connection in series thus the Reuss bound is employed, whereas the Voigt bound is used in the longitudinal and tangential direction due to the parallel connection of plies. Due to the interconnection of individual elements of the effective stiffness matrix, the classical lamination theory described in [20] is used in the case of elasticity. Whereas in the case of moisture diffusivity and thermal conductivity, the Reuss and Voight bounds are sufficient predictions.

In [9] the authors also provide one additional step reflecting the influence of rays. However, due to the low content in the whole wood volume, about 5.9 % [5], their impact on the final properties can be neglected so that this step was omitted from the homogenization procedure.

An example of the application of the homogenization procedure is presented for the following three material properties of the wood: moisture diffusivity, thermal conductivity and elasticity.

6.1 Moisture diffusivity

An easiest computation is in the case of moisture diffusivity. The homogenization procedure starts at the level of earlywood and latewood, because the moisture diffusion properties of individual cell wall constituents have not been found in the literature. Therefore, the first step comprises two phases: cell wall and lumens. The diffusion matrix of the cell wall material is given by Eq. (3.10) as a function of temperature and moisture content. This calculation is limited for cases with moisture content below the fibre saturation point. From that the diffusion of lumens is set equal to that of the moist air which is governed by Eq. (3.16) as a function of the temperature, atmospheric pressure

and relative humidity of surroundings. In [15] the authors use the conversion for diffusivities of phases depending on different concentration gradients. Whereas in this thesis no conversion was employed. The second and also the last step provides the final properties of solid wood employing the standard rules of mixture described earlier. The earlywood and latewood form the laminate. The rays are neglected. The results are summarized in Tab. 15 for the following conditions: 4.5% moisture content, 60% relative humidity, temperature of 20°C. The volume fractions of the lumens of earlywood and latewood, together with the volume fractions of both layers were taken from Tab. 4 for the case of image analysis. The ratios of semi-axes of the ellipsoidal inclusions required for the first step were derived from the lumens dimensions in Tab. 14.

Tab. 15 Diffusion coefficients of spruce wood obtained by homogenization

	D [10^{-12} m^2/s]		
Direction	Radial	Tangential	Longitudinal
Cell wall	0.95	0.95	2.37
Earlywood	5.65	4.80	3819.03
Latewood	1.10	2.00	2895.21
Solid wood	3.09	4.24	3634.27

In [34] the authors state that the moisture diffusion coefficient in the radial direction of Norway spruce is in the order of 10^{-9} m^2/s as related to the moisture content. Radial, tangential and longitudinal diffusion coefficients of *Terminalia superba* at 30°C and zero relative humidity are $1.35x10^{-11}$ m^2/s, $1.16x10^{-11}$ m^2/s and $3.23\ x10^{-11}$ m^2/s, respectively, according to [35]. The resulting value of diffusion coefficient depends on the chosen step of the change of moisture content as it is showed in [36], where the transverse diffusion coefficient of spruce wood is $5.2x10^{-11}$ m^2/s for a cycle from RH=65% to RH=80% and $7.6x10^{-11}$ m^2/s for a cycle from RH=65% to RH=30%, both at a temperature of 20°C. The author also provides the value of the longitudinal diffusivity for a cycle from RH=65% to RH=80%, which is equal to 10^{-9} m^2/s. In [33] the author presents typical values of diffusivity coefficients of Swedish pine and spruce as $1.5x10^{-9}$ m^2/s in the longitudinal direction, $3x10^{-10}$ m^2/s in the radial and tangential direction, determined at RH=75% considering steady-state. Resulting longitudinal diffusion coefficient of solid wood corresponds to that given by the last two authors. The values in the radial and tangential direction are lower, which could be caused by neglection of the rays in the

homogenization model, which provides transport of the water and nutrients in the radial direction. Although there are differences among above-mentioned values, which are not negligible. It could be caused by difficulty of the measurement especially when division into directions is required.

6.2 Thermal conductivity

More demanding calculation is that for the thermal conductivity. The whole homogenization procedure, which is described at the beginning of this chapter, is used to obtain the effective properties at the macroscale. The first step comprises lignin, hemicellulose and water together with extractives, wherein the classical Self-consistent scheme is used.

Tab. 16 Thermal conductivities of spruce wood obtained by homogenization

	$\lambda[W/m.K]$		
	Radial	Tangential	Longitudinal
Polymer network	0.40	0.40	0.40
Cell wall	0.34	0.34	0.63
Earlywood	0.09	0.08	0.21
Latewood	0.21	0.30	0.56
Solid wood	0.10	0.13	0.28

The next step includes two phases namely polymer network corresponding to the effective material from the previous step, and cellulose, where it is not distinguished which type it is, whether amorphous or crystalline. The cellulose is in the form of infinite cylinders, where their deviation from the longitudinal axis corresponds to the MFA. In this step, the Mori-Tanaka method was employed. The thermal conductivities of the cell wall constituents used for the first two steps are summarized in Tab. 10. Their volume fractions were determined according to the computation described at the beginning of Chapter 6. The third step involves the influence of pores, whose properties correspond to the air defined by Eq. (3.19). Their volume fractions and dimensions are the same as for the moisture diffusivity. The Mori-Tanaka method was used again with ellipsoidal inclusions. The last step is the solution of the multi-layered laminate composed of the earlywood and latewood, where the volume fractions of plies are set equal to that obtained

by image analysis, see Tab. 4. The results for the temperature of 20°C, moisture content of 4.5% and zero microfibril angle are summarized in Tab. 16.

The values obtained by homogenization are close to that provided by authors in [4], which are 0.10 W/mK in the transverse direction (radial and tangential) and 0.21 W/mK in the longitudinal direction. In [37] the author determined the longitudinal and transverse thermal conductivity of spruce at 20°C as 0.246 W/mK and 0.111 W/mK, respectively. These values are very similar to the previous ones. Whereas in [38] the thermal conductivity in the longitudinal direction is equal to 0.559 W/mK, which is more than twice as high as the previous mentioned. The same author also provides the value of the transverse thermal conductivity λ=0.107 W/mK, which is quite similar to the others. Both values were measured on Norway spruce specimens at temperature of 20°C. Employing Eqns. (3.17) and (3.18) the values of thermal conductivity for average air-dry density of 441.80 kg/m^3 are thereafter 0.115 W/mK (0.099 kcal/mh°C) and 0.112 W/mK (0.096 kcal/mh°C), respectively. These values are close to that in the transverse direction, whereas lower than the longitudinal conductivity.

6.3 Elasticity

The last example of the homogenization computation is that of the effective mechanical properties of the solid wood. The procedure is the same as in the case of thermal conductivity. The first step provides effective properties of polymer network. The classical Self-consistent scheme with spherical inclusions is employed in this step, where the individual phases are lignin, hemicellulose and water with extractives. The second step comprises polymer network from previous step as a matrix, amorphous and crystalline cellulose as cylindrical inclusions. Cylinders are deviated from the longitudinal axis, where deviation angle is equal to MFA. The Mori-Tanaka method with implemented orientation averaging is used in this step. The volume fractions of the cell wall constituents are computed in the same way as in the case of the thermal conductivity. The properties of individual cell wall constituents are given in Tab. 6. In the third step, the ellipsoidal inclusions corresponding to lumens are inserted into the transversely isotropic matrix, whose properties correspond to that of the cell wall material from previous step. The volume fractions of the lumens for both earlywood and latewood were taken from Tab. 4 for case of image analysis. The ratio of the inclusions semi-axes dimensions are derived from Tab. 14. The lumens act as pores, which reduce the overall

stiffness of the material, from that the properties of lumens are set to zero. The last step covers the influence of the arrangement of the parts of the growth ring, which resembles the laminate. Classical lamination theory is employed to obtain effective mechanical properties of the solid wood, according to the procedure described in [20]. The volume fractions of the earlywood and latewood were set equal to that obtained by the image analysis, see Tab. 4. The results for the moisture content of 4.5% and zero microfibril angle are summarized in Tab. 17.

Tab. 17 Mechanical properties of spruce wood obtained by homogenization

	$E\ [GPa]$			$G\ [GPa]$			$\nu\ [-]$		
	E_R	E_T	E_L	G_{LT}	G_{LR}	G_{RT}	ν_{TR}	ν_{LR}	ν_{LT}
Polymer network	4.92	4.92	4.92	1.83	1.83	1.83	0.35	0.35	0.35
Cell wall	6.88	6.88	39.22	2.28	2.28	2.31	0.49	0.27	0.27
Earlywood	1.02	0.82	12.08	0.38	0.45	0.33	0.31	0.26	0.26
Latewood	3.09	5.88	34.49	1.96	1.18	1.10	0.47	0.26	0.27
Solid wood	1.23	1.84	16.56	0.70	0.51	0.38	0.34	0.26	0.26

The values at the level of cell wall are close to that published by [5], where the axial modulus of the cell wall is equal to 35 GPa and the transverse one to 10 GPa. Small differences between mentioned values, where the longitudinal modulus is higher and the transverse moduli are lower in the case of homogenization, could be caused by MFA. Increase of the angle will reduce the longitudinal value, whereas the transverse ones will increase. Comparing the values of the solid wood obtained by the homogenization Tab. 17 with that given by literature Tab. 5, the longitudinal modulus is in the range mentioned in Tab. 5, while the transverse moduli are higher than that in the table. In [6] the author assesses the longitudinal modulus of spruce, which value of 9.1 GPa is lower than that from homogenization. The same applies to the values given by the author in [4], where the modulus of elasticity of the Norway spruce is 10.2 GPa.

6.4 Sensitivity of the results to changes in input values and assumptions

In this section, the sensitivity of the results to changes in input values are examined. First mentioned is the dependence of the moduli of elasticity in three directions on the

deviation of the crystalline cellulose fibres from the longitudinal axis, where the MFA is changing from 0° to 90°. The elastic moduli were determined by homogenization procedure described in Section 6.3. The volume fractions of the cell wall constituents were computed according to the approach described at the beginning of Chapter 6 for the average moisture content of 4.5 %. Dimensions of the inclusions corresponding to lumens were derived from Tab. 14. The volume fractions of lumens and that of the earlywood and latewood were set constant equal to that in Tab. 4 (image analysis). The resulting dependence is depicted on Fig. 21.

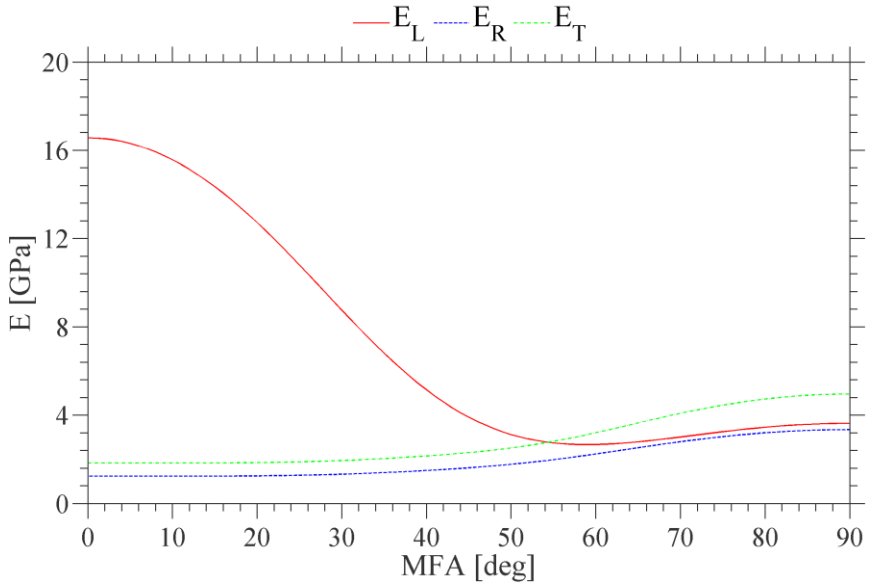

Fig. 21 Dependence of the three moduli of elasticity of wood on MFA

From the course of the variable E_L it is evident that the values are reasonable only up to 60°, approximately. Until this point the value is decreasing, whereas slightly increasing again for MFA higher than 60°. The line expressing modulus in the tangential direction is above that of the radial modulus, which does not comply with the statement that the radial modulus is higher than tangential one proposed by many authors, e.g. Kettunen [5], Persson [13], see also Tab. 5. This could be caused by neglecting the rays in the homogenization procedure or another assumption in the model.

Importance of the proper determination of the lumen volume fraction is demonstrated in the case of the earlywood. The properties were obtained by homogenization up to the level of lumens. The input values were set constant in the same way as in the previous case, except the volume fraction of the earlywood lumens was

assumed to vary. The microfibril angle was considered as zero. The resulting dependence is represented on Fig. 22.

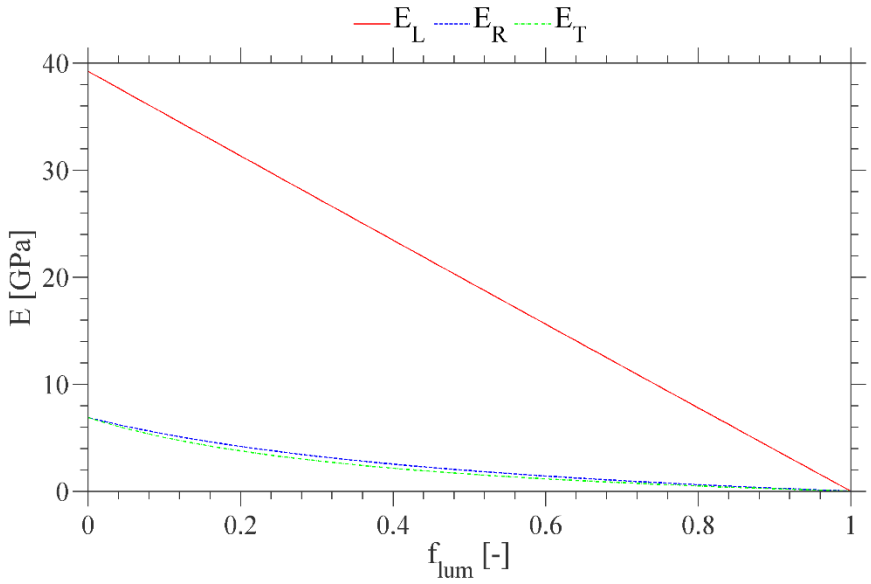

Fig. 22 Dependence of the three moduli of elasticity of the earlywood on the volume fraction of lumens

Clearly the dependence of the longitudinal moduli on the volume fractions of the earlywood lumens seems to be linear. This is not surprising as in the longitudinal direction the Mori-Tanaka predictions for the fibrous composites are identical to simple arithmetic average. Thus, in this case $E_L = (1 - f_{lum})E_{cw,L}$. In contrary, the transversal moduli (radial and tangential) are rather polynomials of higher degree. In addition, all values drop down to zero, when the volume fraction is set equal to 1. Recall that such a result can not be obtained with the Self-consistent method, because it is not recommended to use it for the homogenization of porous composites.

In the case of variable volume fraction of earlywood (Fig. 23), the courses of functions are the same as in the previous case, i.e. the longitudinal modulus corresponds to linear function and that of transverse moduli were higher degree polynomials. The effective properties of wood were determined by the whole homogenization procedure, i.e. to the level of solid wood. The volume fractions of the cell wall constituents were the same as for the previous case. The dimensions of lumens were derived from Tab. 14. The volume fractions of lumens in the earlywood and latewood were set to 0.69 and 0.12, respectively, according to Tab. 4. The volume fraction of earlywood was variable, whereas that of the latewood was computed employing Eq. (6.7). The microfibril angle was set equal to zero.

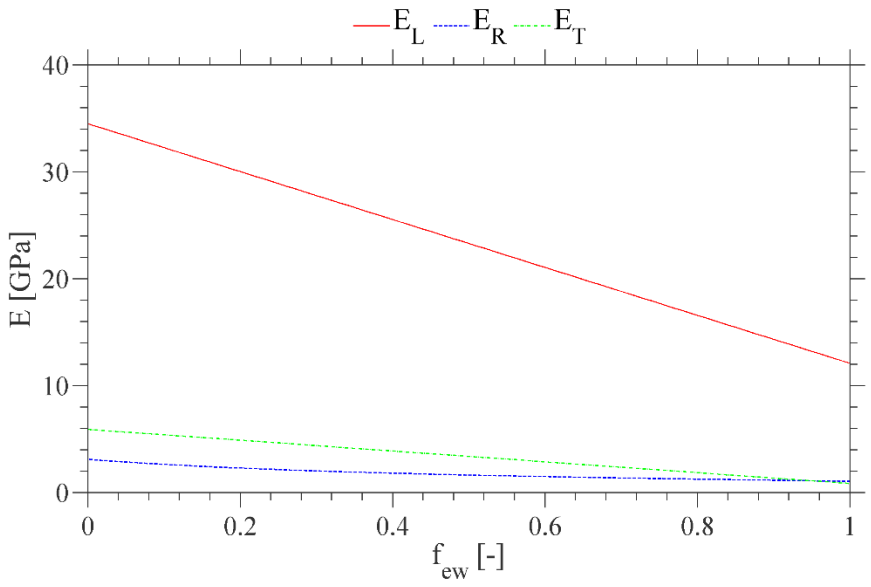

Fig. 23 Dependence of the three moduli of elasticity of wood on the volume fraction of earlywood

The determination of the volume fractions of earlywood and latewood is also very important. The results ranging from 34.49 GPa for $f_{ew}=1$, which corresponds to pure latewood, to 12.08 GPa corresponding to pure earlywood assuming zero microfibril angle. This range is very wide. The figure also shows an interesting phenomenon, where the tangential and radial moduli are getting closer to each other when the volume fraction is approaching to 1. It is probably caused by the different shape of inclusions in both types of wood. Where the latewood lumens are flattened, whereas the earlywood lumens have almost the same dimensions in both directions.

The inclusions at the level of earlywood and latewood are in the form of ellipsoids elongated in the longitudinal direction. The shape is defined by the ratio of the semi-axes, where the ratio of radial : tangential : longitudinal axis dimensions is equal to 0.014:0.011:1 in the case of earlywood and 0.001:0.008:1 in the case of latewood. The influence of changing this ratio on the results of the homogenization procedure is presented for the earlywood as an illustrative example. Characteristics up to the level of cell wall were the same as in the previous cases for the constant moisture content of 4.5%. The volume fraction of lumens was adopted from the image analysis (0.69). The last homogenization step was omitted again. The dependence of the three moduli of elasticity of earlywood on the radial part of the ratio of semi-axes dimensions is depicted on Fig. 24. The value is changing from 0.0012 to 0.0137, where the limits correspond to the latewood and earlywood, respectively.

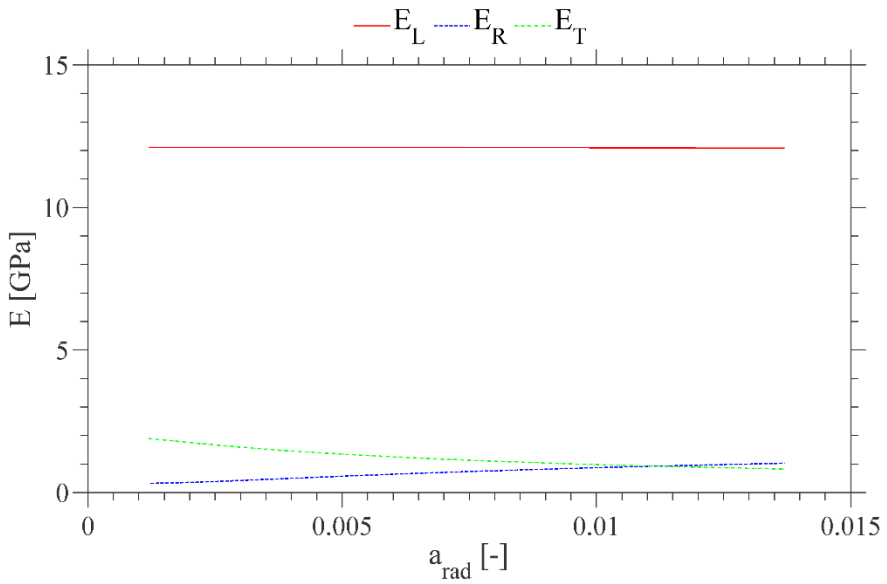

Fig. 24 Dependence of the three moduli of elasticity of earlywood on changing dimension of radial semi-axis

The longitudinal modulus shows only a very slight decrease, from 12.11 GPa to 12.08 GPa. Change of the transversal values are more significant, where the radial modulus varies from 0.31 GPa to 1.02 GPa and the tangential one from 1.88 GPa to 0.82 GPa. This proves the surmise that the converging of both transversal values mentioned in the previous case is due to the shape of inclusions.

Tab. 18 Comparison of effective mechanical properties of wood using different types of inclusions

	$E\ [GPa]$			$G\ [GPa]$			$\nu\ [-]$		
	E_R	E_T	E_L	G_{LT}	G_{LR}	G_{RT}	ν_{TR}	ν_{LR}	ν_{LT}
Ellipsoid	1.23	1.84	16.56	0.70	0.51	0.38	0.34	0.26	0.26
Elliptic cylinder	1.22	1.83	16.63	0.70	0.51	0.38	0.34	0.27	0.27
Circular cylinder	1.13	1.72	16.63	0.69	0.49	0.39	0.36	0.27	0.27
Sphere	1.54	2.08	8.68	0.77	0.58	0.54	0.38	0.24	0.25

Another important assumption seems to be the choice of the inclusion shape. The homogenization procedure was performed in the same way as in the previous cases, with cell wall parameters for MC of 4.5%, volume fractions taken from Tab. 4 obtained by image analysis. The influence of the chosen inclusion shape was examined at the level of earlywood and latewood, i.e. inclusions corresponding to lumens. The resulting values at

the level of solid wood are summarized in Tab. 18, for four types of inclusions, namely ellipsoid, elliptic cylinder, circular cylinder and sphere. Where the ratios of semi-axes of ellipsoids are 0.014:0.011:1 in the case of earlywood and 0.001:0.008:1 in the case of latewood and that of elliptic cylinder are the same, only 1 was replaced by infinity. As it is evident from the table, the results are almost the same for the first three cases, whereas in the case of spherical inclusions the longitudinal modulus is almost half of that first mentioned.

7 Application of homogenization in further study of wood

7.1 Determination of the MFA using nanoindentation

The samples for nanoindentation were prepared in a way the longitudinal direction is practically identical to the longitudinal axis of the cell. From that the indentation modulus E_r supposed to be the same as the longitudinal modulus of the cell wall E_L. However, recall Tab. 17 the value obtained by homogenization is 39.22 GPa, which is almost three times higher than that provided by nanoindentation measurement (13.06 GPa). Although the indentation modulus is not exactly the same as the Young modulus, the difference is still too large. The discrepancy is caused, among other factors, by the microfibril angle, which affects the final mechanical properties. The dependency of the final mechanical properties on the MFA is also depicted on Fig. 21.

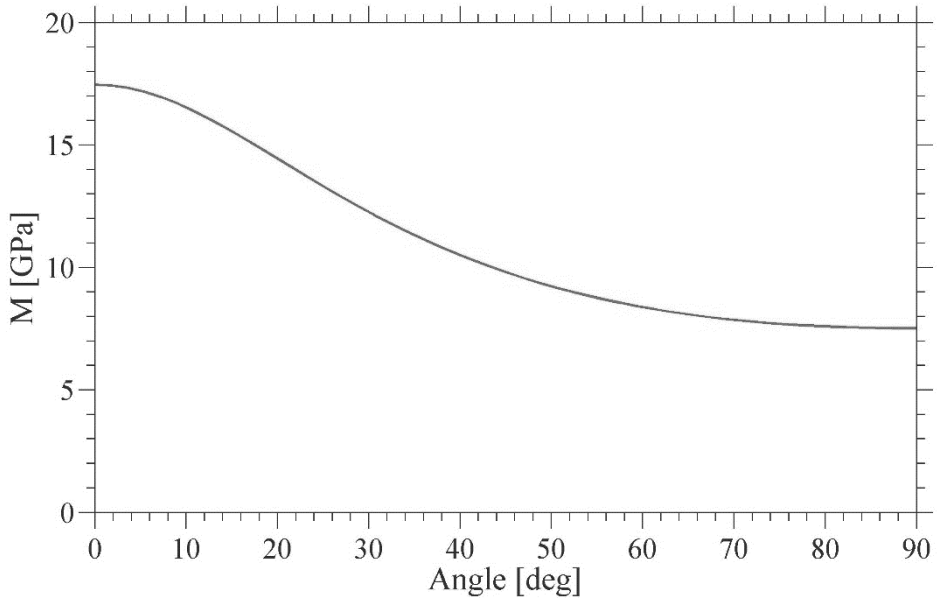

Fig. 25 Angle dependency of the indentation modulus (M)

The effective value from homogenization was derived for zero microfibril angle. To obtain the effective properties at the cell wall level assuming a non-zero MFA, the matrix transformation must be performed. Adopting the anisotropic theory of indentation presented in [39], we acquire indentation modulus as a function of the rotated homogenized stiffness matrix, which corresponds to that obtained by homogenization at the level of cell wall considering the average moisture content of 4.5 %. The variation of

the indentation modulus as a function of deviation from the longitudinal axis is plotted on Fig. 25. Assuming that the deviation angle corresponds to the MFA, it is possible to estimate the microfibril angle simply by comparing the measured values with those derived numerically. Point out, that the theoretical values are expressed in terms of the homogenized stiffness at the cell wall level transformed into the rotated system.

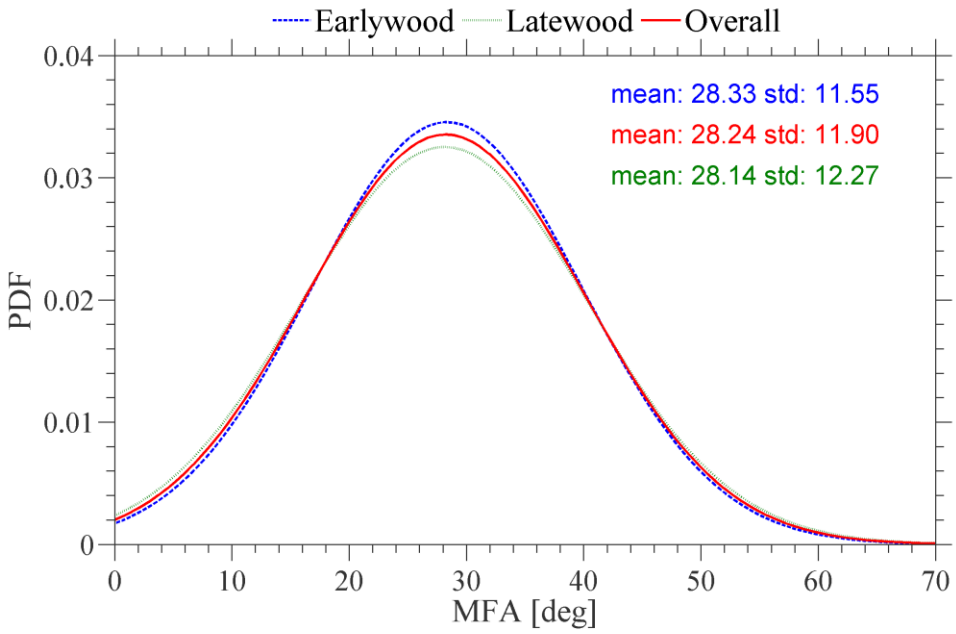

Fig. 26 Probability density function of the microfibril angle

Applying the normal distribution to data, the resulting mean value of the MFA is therefore 28.24°, see Fig. 26. The value is close to the upper limit of the interval 0°-30° stated by [4]. From the calculation, only a slight difference between the earlywood and latewood was observed, whereas referring [40] the MFA of Norway spruce earlywood ranges from 35° to 54° compare to latewood ranging from 3.5° to 11°. The author in [40] also mentioned the MFA of the fast-grown Norway spruce of 29°, which is very close to the present value. In [41] the authors provide MFA of the latewood cell walls of Norway spruce with the mean values of 0°and 20° measured by the X-ray diffraction and corresponding ranges of 0°-11.76°and 14.06°-27.66° obtained by various Raman imaging approaches. However, computed values lay out of range 5°-20° given by [42] for S_2 layer in a mature wood.

Nevertheless, there are many factors affecting the microfibril angle. Firstly, it is the horizontal and vertical position within the stem, where e.g. juvenile wood (in the centre) evinces high values in contrary to mature wood with the lowest values. The difference is

observed among trees even from the same sites. Exposure of the tree to external forces also causes a change in MFA. There are many other aspects given in literature, see e.g. [40; 42].

The whole homogenization procedure was performed again to show the effect of rotation of the fibres on the final properties. The input values remained the same as for the determination of MFA. The whole procedure with used parameters is described in Section 6.3. The results considering the mean value of the microfibril angle (28.24°), see Fig. 26, are summarized in Tab. 19.

Tab. 19 Mechanical properties of spruce obtained by homogenization (MFA=28.24°)

	$E\ [GPa]$			$G\ [GPa]$			$\nu\ [-]$		
	E_R	E_T	E_L	G_{LT}	G_{LR}	G_{RT}	ν_{TR}	ν_{LR}	ν_{LT}
Polymer network	4.92	4.92	4.92	1.83	1.83	1.83	0.35	0.35	0.35
Cell wall	7.03	7.03	22.40	5.55	5.55	2.54	0.38	0.47	0.47
Earlywood	1.07	0.87	6.92	0.93	1.09	0.36	0.27	0.47	0.47
Latewood	3.23	6.02	19.70	4.78	2.87	1.20	0.37	0.47	0.47
Solid wood	1.30	1.92	9.47	1.70	1.25	0.42	0.28	0.47	0.47

When comparing results for zero microfibril angle (Tab. 17) with those considering MFA of 28.24° (Tab. 19), we find out that the influence of the microfibril deviation from longitudinal axis is considerable. The most significant differences are in the direction of wood cells, where the longitudinal modulus of elasticity reduced from 16.56 GPa to 9.47 GPa. On the other hand, the shear moduli in the tangential-longitudinal and radial-longitudinal planes increased to more than double. Also, the Poisson's ratios in the same planes rose. Whereas the radial and tangential elastic moduli show only a slight change. Unfortunately, the rotation of fibres does not have the presumed effect on the effective properties of the cell wall material. The decrease of the longitudinal modulus is marked, while those in the transverse direction almost did not change. These results are even further from the values provided by [5], where the longitudinal modulus is 35 GPa and the transverse one is 10 GPa. The longitudinal modulus of solid wood dropped below the range given in Tab. 5 (13.5-16.7 GPa) and the value obtained by tensile tests (14.29 GPa), see Section 5.4. Nevertheless, it got closer to values stated by [4] (10.2 GPa) and [6] (9.1 GPa), see Section 6.3, where both values were obtained by test in bending.

7.2 Determination of coefficients of hygroexpansion

As it was mentioned in Section 3.3, the wood is a naturally hygroscopic material, i.e. it attracts moisture from surroundings. During drying, the dimensions of the wood element are reduced, i.e. the shrinkage occurs. The opposite phenomenon to shrinkage is swelling, when the wood volume expands with increasing humidity. The ability of the material to change its dimensions in relation to the moisture content is characterized by hygroexpansion coefficient α_h, which is similar to that of the thermal expansion. The effective hygroexpansion coefficient could be implemented to the homogenization procedure. Unfortunately, hygroexpansion properties have not been found for all phases used in the previously mentioned homogenization procedure (Chapter 6) and some phases had different shape than was considered within the homogenization. According to the formula for overall strain:

$$\boldsymbol{\varepsilon} = \boldsymbol{\varepsilon}_e + \boldsymbol{\varepsilon}_h; \quad \boldsymbol{\varepsilon}_h = \boldsymbol{\alpha}_h u \tag{7.1}$$

where $\boldsymbol{\varepsilon}_e$ denotes the elastic strain, $\boldsymbol{\varepsilon}_h$ the hygroexpansion strain, $\boldsymbol{\alpha}_h$ the vector of hygroexpansion coefficients and u the change of moisture content, the effective hygroexpansion coefficients have to be computed simultaneously with the effective mechanical properties. Therefore, the approach described in [13] was adopted for the whole computation. According to this approach, the homogenization is performed in a different way and with different input parameters than the previously mentioned. As it was proposed earlier, the resulting values are strongly dependent on the chosen input parameters. So, it would be appropriate to try another approach with different input values to obtain a comparison of the two procedures.

Apart from the predictions based on the classical micromechanical models, the present sections examine the application of numerical homogenization in the framework of first-order homogenization theory for the sake of comparison.

7.2.1 Analytical homogenization based on Mori-Tanaka method

To avoid difficulties associated with the use of Self-consistent scheme in connection with anisotropic matrices, only the Mori-Tanaka homogenization method is considered. In comparison to Chapter 6, where the S_2 layer was considered only, the prediction of effective coefficients of hygroexpansion follows a different path. This is because both lignin and hemicellulose, unlike crystalline parts of the cellulose, absorb

water quite significantly and as such all layers within the cell wall should be taken into account. In particular, the model assumes the cell wall as a laminate, which consists of three layers: M (middle lamella, primary wall and S_1 layer), S_2 and S_3 layers, recall Section 2.3.

Tab. 20 Mechanical properties of cell wall constituents [13]

	$E\ [GPa]$		$G\ [GPa]$		$\nu\ [-]$	
	$E_R = E_T$	E_L	$G_{LT} = G_{LR}$	G_{RT}	ν_{TR}	$\nu_{LR} = \nu_{LT}$
Lignin	2.75	2.75	1.03	1.03	0.33	0.33
Hemicellulose	3.50	16	1.50	1.25	0.40	0.10
Cellulose	17.50	150	4.50	5.38	0.50	0.01

The first step comprises lignin, hemicellulose and cellulose. The distinction between amorphous and crystalline types of the cellulose is not considered. Further distinction to the original assumptions made in Chapter 3 concerns the material symmetry of cell wall constituent, where the originally isotropic hemicellulose is considered here as transversely isotropic to be consistent with [13]. The elastic properties of individual phases are summarized in Tab. 20 and corresponding coefficients of hygroexpansion are stored in Tab. 21.

Tab. 21 Hygroexpansion coefficients of cell wall constituents [13]

	$\alpha_{h,R}$	$\alpha_{h,T}$	$\alpha_{h,L}$
Lignin	0.351	0.351	0.351
Hemicellulose	1.368	1.368	0.000
Cellulose	0.000	0.000	0.000

Within the cell wall, the cellulose was represented by circular cylindrical inclusions deviated from the longitudinal axis by the angle corresponding to MFA. The value of the microfibril angle of S_2 layer was found with the help of nanoindentation, recall the Section 7.1, whereas the respective values for M and S_3 layers were taken from [13]. As seen from Tab. 22, not only MFA but also the volume fractions of cell wall constituents differ from layer to layer. Note finally, that the volume fractions and properties of phases are assumed to be independent of the moisture content.

The effective mechanical properties were obtained using Eqns. (4.17) and (4.18) in the same way as in Section 6.3. The effective coefficients of hygroexpansion within individual layers were computed by the Levin formula [21] written as:

$$\boldsymbol{\alpha}_h^{hom} = \sum f_r (\mathbf{B}_r^{MT})^T \boldsymbol{\alpha}_{h,r} \tag{7.2}$$

where $r \in \{lignin, hemicellulose, cellulose\}$, $\mathbf{B}_r^{MT}$ is a concentration factor given by Eq. (4.17) for Mori-Tanaka method and $\boldsymbol{\alpha}_{h,r}$ denotes the hygroexpansion coefficient of individual phases. Again, the orientation averaging is implemented to the Mori-Tanaka method to account for every possible position within the cell wall.

Tab. 22 Parameters of individual cell wall layers [13]

	f_{lig}	$f_{hemcell}$	f_{cell}	MFA	$f\ (EW)$	$f\ (LW)$
M	0.65	0.15	0.20	45°	0.352	0.117
S_2	0.24	0.27	0.49	0-45°	0.609	0.870
S_3	0.24	0.27	0.49	75°	0.039	0.013

Using the same approach as in Section 7.1, it is possible to evaluate the microfibril angle of the S_2 layer, considering that nanoindentation results correspond to the properties of this layer. The higher values of the mechanical properties of the S_2 layer considering zero angle led to higher MFA, which is equal to 32.53° comparing to 28.24° (Fig. 26) derived in the previous section.

The second step takes into account the lamellar arrangement of the cell wall. The lamination theory introduced in [20] was used for the computation of the effective mechanical properties in the same way as for solid wood in Section 6.3. The directions were assumed in the similar way as in the case of solid wood, where the radial direction corresponds to the connection in series and the tangential and longitudinal directions to the parallel connection. The volume fractions of individual layers within the cell wall are listed in the last two columns of Tab. 22. Applying this approach to the effective coefficients of hygroexpansion yields the following estimates:

$$\begin{aligned} \alpha_R^{hom} &= \sum f_i\ \alpha_{h,R,i} \\ \alpha_T^{hom} &= \frac{\sum f_i\ E_{T,i}\ \alpha_{h,T,i}}{\sum f_i\ E_{T,i}} \end{aligned} \tag{7.3}$$

$$\alpha_L^{hom} = \frac{\sum f_i \, E_{L,i} \, \alpha_{h,L,i}}{\sum f_i \, E_{L,i}}$$

where $i \in \{$*M layer, S₂ layer, S₃ layer*$\}$, E is the elastic modulus and R, T, L denote to the radial, tangential and longitudinal direction. The resulting values of the effective mechanical properties are summarized in Tab. 23 and those of the effective hygroexpansion coefficients are in Tab. 24.

Tab. 23 Mechanical properties of spruce obtained by homogenization according to [13]

	$E\ [GPa]$			$G\ [GPa]$			$\nu\ [-]$		
	E_R	E_T	E_L	G_{LT}	G_{LR}	G_{RT}	ν_{TR}	ν_{LR}	ν_{LT}
M layer	5.20	5.20	6.26	5.85	5.85	2.53	0.03	0.55	0.55
S_2 layer *	7.69	7.69	32.18	13.23	13.23	3.39	0.14	0.76	0.76
S_3 layer	32.71	32.71	6.68	5.77	5.77	13.78	0.19	0.10	0.10
Earlywood cell wall	7.26	8.05	22.95	10.34	8.85	3.11	0.15	0.68	0.61
Latewood cell wall	7.60	7.86	29.61	12.27	11.36	3.29	0.15	0.73	0.71

*MFA=32.53°

It should be noted that the computation leads to different elastic properties of the earlywood and latewood cell wall, as it is evident from Tab. 23. This contradicts the results from Section 5.5, where the S_2 layer only was considered in the homogenization thus suggesting the same cell wall stiffness of both the earlywood and latewood.

Tab. 24 Hygroexpansion coefficients of spruce obtained by homogenization according to [13]

	$\alpha_{h,R}$	$\alpha_{h,T}$	$\alpha_{h,L}$
M layer	0.363	0.363	0.248
S_2 layer *	0.363	0.363	0.125
S_3 layer	0.228	0.228	0.396
Earlywood cell wall	0.358	0.341	0.141
Latewood cell wall	0.361	0.356	0.129

*MFA=32.53°

Although the microfibril angle is higher, the resulting values at the level of cell wall are also higher than that mentioned in Tab. 19. It could be caused by higher volume

fraction of cellulose with large longitudinal modulus. Even though the total volume fraction is approximately the same in both cases, in the previously mentioned procedure, the cellulose is divided into crystalline with high stiffness and amorphous with very low values of longitudinal modulus. Also, the assumption of the transversely isotropic hemicellulose with higher longitudinal modulus may have appreciable impact on final properties.

The next step covers the influence of the wood porosity. In order to make the comparison between the numerical and analytical solutions, the same assumptions as for the numerical homogenization were adopted. The effective properties at the level of lumens were computed using the same procedure as in the first step described at the beginning of this section. The inclusions in the form of elliptic cylinders aligned in the longitudinal direction were embedded in the matrix with properties of the cell wall material. Recall that in Chapter 6 the inclusions were assumed to be of ellipsoidal shape. The dimensions and volume fractions of the lumens were derived from Fig. 27. Subsequently, the volume fraction of lumens in the earlywood is 0.86 and 0.21 in the latewood. The results are compared with those obtained by numerical homogenization in Tab. 25.

7.2.2 Numerical homogenization up to level of lumens

The present section provides the derivation of the effective mechanical properties and coefficients of hygroexpansion to be compared with the Mori-Tanaka predictions derived in Section 7.2.1. This approach is based on the application of periodic unit cell (PUC).

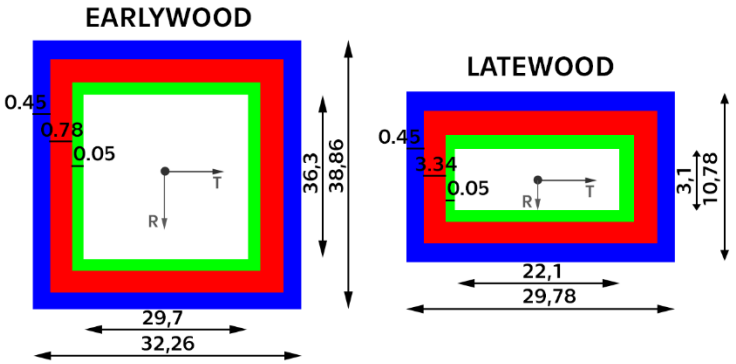

Fig. 27 Geometry of PUC of earlywood and latewood cell

The PUC is defined for earlywood and latewood separately to distinguish between the different dimensions of the cells and lumens and volume fractions of the individual

layers within the cell wall. Similar to the previous section, three layers of the cell wall are considered as follows: M layer comprising middle lamella, primary wall and S_1 layer (blue), S_2 layer (red) and S_3 layer (green). The simplified geometry of PUCs is depicted on Fig. 27, see also [13].

Owing to the fact that the evaluation of effective coefficients of hygroexpansion is similar to that of thermal expansion, we follow the procedure described in [22] and assume the PUC to be loaded by uniform tractions compatible with macroscopically uniform stress $\boldsymbol{\Sigma}$ and a uniform moisture change u. The local constitutive law then reads:

$$\boldsymbol{\sigma}(\boldsymbol{x}) = \mathbf{L}(\boldsymbol{x})(\boldsymbol{\varepsilon}(\boldsymbol{x}) - \boldsymbol{\alpha}_h(\boldsymbol{x})u) \tag{7.4}$$

where $\mathbf{L}$ is the local stiffness matrix, $\boldsymbol{\alpha}_h$ comprises the coefficients of hygroexpansion and u denotes the change of the moisture content. In the framework of first order homogenization, the local strain $\boldsymbol{\varepsilon}(\boldsymbol{x})$ is split into a macroscopic part $\boldsymbol{E}$ constant over the PUC and a fluctuation part $\boldsymbol{\varepsilon}^*(\boldsymbol{x})$ such that:

$$\boldsymbol{\varepsilon}(\boldsymbol{x}) = \boldsymbol{E} + \boldsymbol{\varepsilon}^*(\boldsymbol{x}) \tag{7.5}$$

It is obvious that the fluctuation part has to disappear during volume averaging. This could be achieved by assuming the fluctuation part $\boldsymbol{\varepsilon}^*$to be periodic so that the corresponding displacement field $\boldsymbol{u}^*$ is subjected to specific periodic boundary conditions, see [22] for further details.

The finite element formulation is based on the application of the Hill Lemma written as:

$$\langle \delta\boldsymbol{\varepsilon}(\boldsymbol{x})^T \boldsymbol{\sigma}(\boldsymbol{x}) \rangle = \delta \boldsymbol{E}^T \boldsymbol{\Sigma} \tag{7.6}$$

where angle brackets denote the volume average. Substituting Eqns. (7.4) and (7.5) into Eq. (7.6) yields:

$$\begin{aligned} \delta \boldsymbol{E}^T \langle \mathbf{L}(\boldsymbol{x})(\boldsymbol{E} + \boldsymbol{\varepsilon}^*(\boldsymbol{x}) - \boldsymbol{\alpha}_h(\boldsymbol{x})u) \rangle + \langle \delta\boldsymbol{\varepsilon}^*(\boldsymbol{x})^T \mathbf{L}(\boldsymbol{x})(\boldsymbol{E} + \\ \boldsymbol{\varepsilon}^*(\boldsymbol{x}) - \boldsymbol{\alpha}_h(\boldsymbol{x})u) \rangle = \delta \boldsymbol{E}^T \boldsymbol{\Sigma} \end{aligned} \tag{7.7}$$

Since $\delta\boldsymbol{E}$ and $\delta\boldsymbol{\varepsilon}^*(\boldsymbol{x})$ are independent, the preceding equation can be split into two statements:

$$\begin{aligned} \delta \boldsymbol{E}^T \boldsymbol{\Sigma} &= \delta \boldsymbol{E}^T [\langle \mathbf{L}(\boldsymbol{x}) \rangle \boldsymbol{E} + \langle \mathbf{L}(\boldsymbol{x}) \boldsymbol{\varepsilon}^*(\boldsymbol{x}) \rangle - \langle \mathbf{L}(\boldsymbol{x}) \boldsymbol{\alpha}_h(\boldsymbol{x}) u \rangle] \\ 0 &= \langle \delta \boldsymbol{\varepsilon}^*(\boldsymbol{x})^T \mathbf{L}(\boldsymbol{x}) \rangle \boldsymbol{E} + \langle \delta \boldsymbol{\varepsilon}^*(\boldsymbol{x})^T \mathbf{L}(\boldsymbol{x}) (\varepsilon^*(\boldsymbol{x}) - \boldsymbol{\alpha}_h(\boldsymbol{x}) u) \rangle \end{aligned} \tag{7.8}$$

Upon the finite element discretization the strain field becomes:

$$\boldsymbol{\varepsilon}(\boldsymbol{x}) = \boldsymbol{E} + \mathbf{B}(\boldsymbol{x}) \boldsymbol{r} \tag{7.9}$$

where $\mathbf{B}$ is the geometric matrix and $\boldsymbol{r}$ is the vector of nodal displacements of the fluctuation part of the displacement field. Combining Eqns. (7.8) and (7.9) provides the discretized system of algebraic equations:

$$\begin{bmatrix} \frac{1}{\Omega}\int_\Omega \mathbf{L}\, \mathrm{d}\Omega & \frac{1}{\Omega}\int_\Omega \mathbf{L}\mathbf{B}\, \mathrm{d}\Omega \\ \frac{1}{\Omega}\int_\Omega \mathbf{B}^T\mathbf{L}\, \mathrm{d}\Omega & \frac{1}{\Omega}\int_\Omega \mathbf{B}^T\mathbf{L}\mathbf{B}\, \mathrm{d}\Omega \end{bmatrix} \begin{Bmatrix} \boldsymbol{E} \\ \boldsymbol{r} \end{Bmatrix} = \begin{Bmatrix} \mathrm{E} + \frac{1}{\Omega}\int_\Omega \mathbf{L}\boldsymbol{\alpha}_h u\, \mathrm{d}\Omega \\ \frac{1}{\Omega}\int_\Omega \mathbf{B}^T\mathbf{L}\boldsymbol{\alpha}_h u\, \mathrm{d}\Omega \end{Bmatrix} \tag{7.10}$$

where the macroscopic strain $\boldsymbol{E}$ and the nodal fluctuation displacements $\boldsymbol{r}$ are unknown quantities, which can be solved by these equations.

Finally, setting the macroscopic stress $\boldsymbol{\Sigma} = 0$ and the moisture change $u = 1$ yields the effective coefficients of hygroexpansion at the level of lumens as the components of the macroscopic strain $\boldsymbol{E}$.

Tab. 25 Comparison of results from analytical and numerical homogenization at level of lumens

		$\mathbf{L}_{11}$	$\mathbf{L}_{22}$	$\mathbf{L}_{33}$	$\alpha_{h,R}$	$\alpha_{h,T}$	$\alpha_{h,L}$
Numerical	- EW	0.74	0.61	3.71	0.356	0.357	0.143
	- LW	2.65	6.90	28.45	0.369	0.363	0.130
Analytical	- EW	0.55	0.46	3.77	0.358	0.341	0.141
	- LW	2.67	7.10	29.32	0.361	0.356	0.129

The results from the numerical homogenization assuming plain-strain are compared with those derived from analytical homogenization in Tab. 25, where $\mathbf{L}_{nm}$ denotes the element of the stiffness matrix and α_h is the coefficient of hygroexpansion in a given direction. Furthermore, the subscripts refer to the direction as follows: 11 – radial, 22 – tangential, 33 – longitudinal. The presented values obtained by both approaches are very

similar. Slightly larger differences, but still insignificant, are among the transverse elements of the stiffness matrix.

8 Conclusion

The wood is a widely used building material. The major part of timber used for building construction in the Czech Republic comprises the Norway spruce (*Picea abies*), therefore the thesis is mainly concerned about this species. The use of wood is considerably limited, because of its heterogeneity and almost unpredictable mechanical properties. For a full understanding of the behaviour of wood it is necessary to know the influences, which affect its mechanical and transport properties.

It is important to understand the wood composition and its behaviour in a green state, i.e. to understand the behaviour of the tree itself. It is useful to know the impact of the growth conditions on the final properties (Section 2.4). This knowledge can simplify the following research. In this case, the tree stem, from which the timber is mainly produced, is studied. First, it is necessary to introduce three basic directions, which are consistent with a concentric arrangement of the growth rings. The radial direction runs from the centre of the stem to the periphery and is perpendicular to the growth rings. The tangential direction is in the direction of the tangent to growth rings. The longitudinal (or axial) direction is assumed along the stem. Basically, the wood is mainly composed of tracheids, the long tube-like cells, which are different in the earlywood and latewood. The earlywood cells are large, where thin cell walls surround wide lumens (cavity inside the cell). They are formed at the beginning of the growth season and act as conductors of water and nutrients. On the other hand, the latewood cells are narrower in the radial direction with thick walls and thin lumens. These cells are formed at the end of the growth season, mainly to provide support to the whole tree and storage of nutrients. The earlywood and latewood together form the growth ring, which resembles lamellar arrangement. The same also applies to the cell wall, where the layers are arranged as follows (describing outwards): warty layer, secondary wall (divided into inner, middle and outer layer) and primary wall. The adjacent cell walls are bonded together by middle lamella. The most significant effect on the overall strength of the cell wall has the middle layer of the secondary wall (S_2 layer), due to the parallel arrangement of the microfibrils and its large volume fraction within the cell wall. Furthermore, the cell wall is composed of cellulose (crystalline and amorphous), hemicellulose, lignin and extractives. The cellulose occurs in the form of microfibrils – long fibres with the core of the crystalline cellulose surrounded by the amorphous cellulose and hemicellulose, bonded together by

lignin. It is proposed by many authors that the deviation of the microfibrils from the longitudinal axis (denoted as the microfibril angle – MFA) has a significant influence on the properties of the cell wall and subsequently on the overall mechanical behaviour. The structural composition of wood is more elaborated in Chapter 2.

The prerequisite for a proper structural design is the knowledge of the mechanical properties of the material. The basic quantity determining whether the wood is weaker or stronger is the density. There are several types of densities of which the most used are the oven-dry and air-dry density, see Section 3.1. The range of the oven-dry density obtained by the measurements within this thesis is 365.34-510.23 kg/m^3, see Section 5.1. It corresponds to the interval stated in [13], where the density of clear wood specimens of Norway spruce falls within the range of 350-600 kg/m^3. The density is inversely proportional to the amount of pores, where higher porosity indicates lower density and subsequently lower strength of the material. Thus, it is essential to determine the exact distribution and dimensions of pores. Recalling the cell structure, where larger pores occur mainly in the earlywood, an accurate determination of the volume fractions of the earlywood and latewood is also necessary. Both characteristics can be determined by various methods, whereas the values presented in this thesis are mainly obtained by image analysis, see Sections 5.2 and 5.3. In Section 3.1, the computation of the volume fractions of the earlywood and latewood together with that of lumens (pores) according to [9] and [10] was introduced, whereas it was proved (Sections 5.2 and 5.3) that these relationships depending on the density do not express the reality quite well. The measurements of the widths of growth rings and their parts show the dependency of the earlywood width on the density, while the latewood widths seem to be rather constant of about 0.2 mm. Similar conclusion has been put forward in [13]. Independence of the density has been observed also in the case of lumen volume fractions. For almost all computations, the average values obtained by image analysis were considered, where the volume fractions of the earlywood and latewood are 0.8 and 0.2, respectively, and the volume fractions of lumens are 0.69 in the earlywood and 0.12 in the latewood, see Tab. 4.

The ability of the material to resist external forces is represented by mechanical properties, see Section 3.2. The stress level at which failure occurs is considered as strength varying in dependence on the manner of loading. Elastic behaviour can be characterized by the set of 12 constants, where nine are independent considering orthotropy of the wood. These parameters can be determined either experimentally or

numerically. Probably, the most fundamental quantity describing the elastic behaviour of the material is the modulus of elasticity. According to [6], more accurate values of the MOE could be obtained by the axial tension tests. The tensile test performed within this thesis is described in Section 5.4, where the mean value is 14.29 GPa, which falls within the range given in Tab. 5. The mechanical properties could be measured even on lower scales. It is proposed by many authors that the main load bearing wood constituent is the cell wall. Therefore, it could be useful to know the mechanical properties of the cell wall. These can by measured directly by nanoindentation. The basic principle of the nanoindentation experiment is pushing the small hard tip with known geometry and mechanical properties into the tested material with unknown properties while simultaneously recording the load and indentation depth relative to the initial undeformed surface. The method, basic equations and the measurements itself are further described in Section 5.5. The measured data have to be evaluated by various approaches, in this case the anisotropic theory of indentation presented in [39] was employed. Due to the assumption that the overall strength of the cell wall is governed by that of the S_2 layer, all indents were localized into this layer. Based on the results depicted on Fig. 19, it is assumed that the properties of the cell wall are the same throughout the whole growth ring. The mean value of the indentation modulus is 13.06 GPa, whereas it is necessary to point out that it does not correspond to the Young modulus of the material.

The wood is a naturally hygroscopic material, i.e. it attracts moisture from surrounding atmosphere. However, the presence of the water affects all other properties. The water is present in the wood in two forms: free water (i.e. liquid water or water vapour in the lumens and other cavities) and bound water (i.e. liquid water in the cell wall) [5]. The amount of water present in wood is characterized by the moisture content (MC), defined as a ratio of the mass of water to the oven-dried wood mass. The moisture content belongs to the most relevant quantities, which have to be measured during the material examination. The basic method of moisture content determination is based drying and weighing, where the wood sample is weighed before and after drying in an oven. The gravimetric moisture content is therefore computed by Eq. (3.8). The mean value of MC of samples examined within this thesis, see Section 5.1, is 4.5%. There are two important values of MC: the equilibrium moisture content (EMC) defined under constant conditions and the fibre saturation point (FSP) referring to the state, when the cell walls are fully saturated and there is no free water in lumens. The average value of FSP is about 30%

[3]. This point is very important, because below FSP, most properties change as a function of MC and so the dimensions (i.e. shrinkage occurs). Also, below FSP the motion changes into diffusion only. There are two types of motion obeying Fick's first law: flow along the lumens, driven by difference of pressures, and diffusion along lumens or through cell wall dependent on a concentration gradient. Considering the steady-state diffusion, the macroscopic moisture flux is governed by Eq. (3.9). In this equation, the material property is characterized by moisture diffusion coefficient D [m^2/s], which could be also measured e.g. by cup method. Unfortunately, the measurement described in Section 5.6 led to values too far from those stated in the literature. Therefore, they were not included in further data processing.

Nowadays, a proper building design can not be managed without the knowledge of thermal properties (see Section 3.4). One of the key quantities is the coefficient of thermal conductivity λ [W/mK]. It characterizes the resistance of the material to the passage of heat and is governed by Fourier's law. The thermal conductivity is also influenced by moisture, such as the other material properties. According to [4] the values for spruce with density of 340 kg/m^3 are 0.10 W/mK in the transverse direction and 0.21 W/mK in the longitudinal direction.

All mentioned material characteristics could be determined computationally, e.g. by micromechanical homogenization. Homogenization methods are used for the computation of the effective properties of the heterogeneous material, especially composites, based on the knowledge of the structural composition and the material properties of all constituents. An overview of methods and the derivation of individual equations are mentioned in Chapter 4. The wood resembles the natural composite and could be treated as such. Recalling the structural composition described in Chapter 2 the most appropriate approach of the determination of effective properties seems to be an upscale homogenization starting from the level of cell wall constituents up to the level of solid wood (Chapter 6). Adopting the approach described in [9] the homogenization procedure comprises several steps. The effective material obtained by the first step is called polymer network and consists of three phases: lignin, hemicellulose and water with extractives forming one phase. Lignin and hemicellulose are almost of the same volume fractions and the role of the matrix and inclusion is not clear. Therefore, the Self-consistent scheme with spherical inclusions seems to be a good choice. The next step provides the effective properties of the cell wall. Circular cylindrical inclusions,

corresponding to cellulose or amorphous and crystalline cellulose separately, are inserted into the isotropic matrix (polymer network from the previous step). Within this step the influence of the microfibril angle is implemented as a deviation of inclusions from the longitudinal axis (axis x_3 in this thesis). These assumptions lead to the Mori-Tanaka method for isotropic matrix with infinite circular cylindrical inclusions deviated by MFA. This step also includes the orientation averaging to obtain transversely isotropic material. The third step covers the influence of the porous structure. According to the wood composition, see Section 2.2, the shape of pores (lumens) could be simplified into the form of ellipsoidal cavities, which are different in the case of earlywood and latewood. The matrix formed by the cell wall is weakened by pores. The Mori-Tanaka method with ellipsoidal inclusions oriented in the longitudinal direction in transversely isotropic matrix was employed for the computation of the effective properties. Mainly because, unlike the Self-consistent scheme, this method is well suitable for materials with porous phase. The last step covers the influence of the arrangement of the earlywood and latewood parts of the growth ring, which resembles the multi-layered laminate. The classical lamination theory described in [20] was employed in the case of elasticity, whereas the Voight and Reuss bounds governed by Eqns. (4.12) and (4.13) give sufficient estimates in the case of moisture diffusivity and thermal conductivity. In [9] the authors also provide one additional step reflecting the influence of rays. Whereas this step was omitted from the procedure due to the low content of the rays in the whole wood volume, about 5.9% [5].

The homogenization procedure was performed for the case of elasticity, moisture diffusivity and thermal conductivity. In the case of the moisture diffusivity the homogenization procedure starts at the level of lumens, whereas the thermal conductivity and elasticity were computed employing the whole procedure. The application of the homogenization procedure together with properties of individual phases for the three cases are described in Sections 6.1, 6.2 and 6.3. The volume fractions of the cell wall constituents were the same for all cases and were derived according to the approach described at the beginning of Chapter 6 for the moisture content set equal to 4.5%. The volume fractions of the earlywood (0.80) and latewood (0.20) and that of the lumens in the earlywood (0.69) and latewood (0.12) were taken from Tab. 4 for the case of image analysis. The microfibril angle was considered equal to zero.

According to Tab. 15 the resulting diffusion coefficients of spruce at the level of solid wood are 3.09×10^{-12} m^2/s (radial), 4.24×10^{-12} m^2/s (tangential) and 3634.27×10^{-12} m^2/s (longitudinal). The value in the longitudinal direction correspond to that given in [33], where the author presents typical values of diffusivity coefficients of Swedish pine and spruce as 1.5×10^{-9} m^2/s in the longitudinal direction, 3×10^{-10} m^2/s in the radial and tangential direction, determined at RH=75% considering steady-state. Whereas the values in the transverse direction obtained by homogenization are considerably lower. Although, the values are not consistent among published results. In [34] the authors state that the moisture diffusion coefficient in the radial direction of Norway spruce is in the order of 10^{-9} m^2/s as related to the moisture content. On the other hand, in [36] the author presents the transverse diffusion coefficient of spruce wood in relation to the chosen step of the change of moisture content, where the resulting values are 5.2×10^{-11} m^2/s for a cycle from RH=65% to RH=80% and 7.6×10^{-11} m^2/s for a cycle from RH=65% to RH=30%, both at a temperature of 20°C. The author also provides the value of the longitudinal diffusivity for a cycle from RH=65% to RH=80%, that is equal to 10^{-9} m^2/s, which corresponds to that obtained by homogenization too. However, it should be mentioned, that the measurement is very difficult, especially when division into directions is required.

The results of the homogenization for the case of the thermal conductivity are summarized in Tab. 16. The coefficients of thermal conductivity at the level of solid wood are 0.10 W/mK (radial), 0.13 W/mK (tangential) and 0.28 W/mK (longitudinal). These values are close to that provided by the authors in [4], where the transverse coefficient is 0.10 W/mK and the longitudinal one is 0.21 W/mK. The similar values are provided also in [37], where the thermal conductivity of spruce at 20°C is 0.111 W/mK in the transverse direction and 0.246 W/mK in the longitudinal direction. On the other hand, in [38] the authors present considerably higher value of the longitudinal coefficient (0.559 W/mK), whereas the transverse thermal conductivity is 0.107 W/mK, which is similar to those previously mentioned.

The effective values of the mechanical properties at all levels of the homogenization procedure are summarized in Tab. 17. The effective Young moduli at the level of solid wood are 1.23 GPa in the radial direction, 1.84 GPa in the tangential direction and 16.56 GPa in the longitudinal direction. Comparing to Tab. 5, the longitudinal modulus obtained by homogenization falls within the range of 13.5-16.7 GPa given by [13]. Whereas the values corresponding to the radial and tangential directions are quite higher

than that mentioned in Tab. 5 (0.70-0.90 GPa – radial, 0.40-0.65 GPa – tangential). The longitudinal modulus is close to that measured in axial tension test, where the mean value is 14.29 GPa, see Section 5.4. Although, the homogenization gives higher estimate than values given by [6] and [4], where the longitudinal moduli are 9.1 GPa and 10.2 GPa, respectively. Also, the values at the level of cell wall are slightly different than that published in the literature. For example, in [5] the axial modulus of the cell wall is 35 GPa and the transverse one is 10 GPa. The small differences between mentioned values, where the longitudinal modulus is higher and the transverse moduli are lower in the case of homogenization, could be caused by the deviation of microfibrils.

Based on the previously mentioned results, it is possible to propose that the homogenization provides more or less reasonable estimates of the effective thermal conductivity and values in the longitudinal direction of the remaining quantities. The discrepancy could be caused by many factors. There could be inaccuracies in the homogenization procedure (e.g. wrong input values, improperly conceived model etc.) or even the measurement and adopted assumptions within the data evaluation can lead to misleading results. The values in previous paragraphs show a great variability in data reported in the literature. However, the improvement of measurement methods is not a subject of this thesis. The effect of change in some input values and assumptions on resulting effective properties is examined in Section 6.4, where the effect on mechanical properties only was studied for the sake of simplicity.

The presented variations in input values in Section 6.4 show that the choice of the inclusion shape, see Tab. 18, has only a little effect on the final properties, except the spherical inclusion that was chosen only as an illustrative case and does not correspond to the real shape of lumens. Increasing radial semi-axis dimension leads to the change in transverse effective moduli, whereas the longitudinal modulus remains almost unchanged. The dependency is depicted on Fig. 24. More significant is the influence of the volume fractions of parts of the growth ring, i.e. earlywood and latewood (Fig. 23). With increasing volume fraction of the earlywood, the mechanical properties are changing from that of pure latewood to the pure earlywood, where the values decrease from 34.49 GPa to 12.08 GPa considering zero MFA. Referring to Fig. 22, the most significant is the influence of the wood porosity. The reduction of mechanical properties due to increasing volume fraction of pores is considerable. Thus, the proper determination of the lumens volume fraction is a key factor determining the accuracy of final results.

It is proved by many authors that the microfibril angle has a significant impact on overall mechanical properties. It is possible to implement it into the homogenization procedure as the deviation of inclusions within the second step. The dependency of the three moduli at the level of solid wood on the deviation angle is depicted on Fig. 21. As it is evident from the picture, the MFA mainly affects the longitudinal modulus, where the most significant decrease is between 0° and 50°. Considering that the values measured by nanoindentation correspond to the real properties of the cell wall, it is possible to adopt an inverse approach and estimate the MFA by combining the homogenization and nanoindentation results, see Section 7.1.

Tab. 26 Mechanical properties obtained by homogenization for two different values of MFA

	MFA	$E\ [GPa]$			$G\ [GPa]$			$\nu\ [-]$		
	[°]	E_R	E_T	E_L	G_{LT}	G_{LR}	G_{RT}	ν_{TR}	ν_{LR}	ν_{LT}
Cell wall	0	6.88	6.88	39.22	2.28	2.28	2.31	0.49	0.27	0.27
	28.24	7.03	7.03	22.40	5.55	5.55	2.54	0.38	0.47	0.47
Solid wood	0	1.23	1.84	16.56	0.70	0.51	0.38	0.34	0.26	0.26
	28.24	1.30	1.92	9.47	1.70	1.25	0.42	0.28	0.47	0.47

Recalling the results of both methods, the effective longitudinal modulus obtained by homogenization for zero MFA is 39.22 GPa, whereas the indentation modulus measured by nanoindentation (13.06 GPa) is almost three times lower. It is evident that the matrix transformation has to be employed to obtain the effective properties of the cell wall for a non-zero MFA. Adopting the anisotropic theory of indentation presented in [39], we acquire the indentation modulus as a function of the rotated homogenized stiffness matrix. The dependency of the indentation modulus on the deviation angle is depicted on Fig. 25. Comparing the measured values with those derived numerically, it is possible to estimate the microfibril angle. Considering the normal distribution of data in Fig. 26, the mean value of the microfibril angle is 28.24°. This value is close to the upper limit of the interval 0°-30° presented in [4]. On the basis of the nanoindentation measurements, it was assumed that the cell wall has the same properties regardless of its position within the growth ring. Whereas, when referring to [40] the MFA of Norway spruce earlywood ranges from 35° to 54° compare to latewood ranging from 3.5° to 11°. Close to the computed value is the MFA of the fast grown Norway spruce (29°) stated in [40]. However, they lay out of range 5°-20° given by [42] for S_2 layer in a mature wood.

Nevertheless, there are many factors affecting the microfibril angle, see e.g. [40; 42]. The effect of the deviation of the reinforcing fibres is showed in Tab. 26, where the results from the homogenization procedure at the level of cell wall and solid wood are presented as a combination of Tab. 17 and Tab. 19. Unfortunately, the rotation of fibres does not have the presumed effect on the effective properties. The longitudinal moduli decreased significantly, while the radial and tangential moduli increased rather slightly. The longitudinal modulus of the cell wall is considerably lower than that provided by [5] (35 GPa). At the level of solid wood, the longitudinal modulus dropped below the range given in Tab. 5 (13.5-16.7 GPa) and the value obtained by the tensile tests (14.29 GPa), see Section 5.4. But it got closer to values stated in [4] (10.2 GPa) and [6] (9.1 GPa), see Section 6.3, where both values were obtained by the bending test.

The wood is a naturally hygroscopic material that receives water from its surroundings. During drying, the dimensions of the wood element are reduced, i.e. the shrinkage occurs. The opposite phenomenon to shrinkage is swelling, when the wood volume expands with increasing humidity. The ability of the material to change its dimensions in relation to the moisture content is characterized by the coefficient of hygroexpansion α_h, which is similar to that of the thermal expansion. The coefficients of hygroexpansion could be determined also by homogenization. Due to the connection of the elastic and hygroexpansion strain, see Eq. (7.1), these two quantities have to be solved simultaneously. Unfortunately, the hygroexpansion properties of all phases of the homogenization procedure have not been found. Therefore, the approach described in [13] was adopted. According to this approach, the homogenization is performed in a different way and with different input parameters and assumptions than that previously mentioned. As it was proposed earlier, the resulting values are strongly dependent on the chosen input parameters, so it provides a comparison to the homogenization procedure described in Chapters 4 and 6. Apart from the predictions based on the classical micromechanical models, the numerical homogenization is examined within this chapter. The analytical homogenization is based on the Mori-Tanaka method. In comparison to Chapter 6, where the S_2 layer is considered only, all layers within the cell wall are accounted for, recall the cell wall composition in Section 2.3. Each layer is considered as fibre-reinforced composite comprising lignin, hemicellulose and cellulose, where the last two phases are in the form of circular cylindrical inclusions deviated from the longitudinal axis by MFA. The distinction between amorphous and crystalline types of the cellulose

is not considered. Further distinction to the original assumptions made in Chapter 3 concerns the material symmetry of cell wall constituents, where originally isotropic hemicellulose is considered here as transversely isotropic to be consistent with [13]. The properties and volume fractions of individual phases are summarized in tables within Section 7.2.1. The effective properties of cell wall layers were computed by the Mori-Tanaka method employing the Levin formula in the case of hygroexpansion. Using the same approach as in Section 7.1, it is possible to evaluate the microfibril angle of the S_2 layer, considering that nanoindentation results correspond to the properties of this layer. The calculation led to the resulting MFA being equal to 32.53°, which is higher than 28.24° obtained in Section 7.1. As it was mentioned earlier, the cell wall resembles laminate. Therefore, the lamination theory introduced in [20] and Eqns. (7.3) were used for the computation of the effective properties of the whole cell wall. The directions were assumed in the same way as in the case of the solid wood, where the radial direction corresponds to the connection in series and the tangential and longitudinal directions to the parallel connection. The resulting properties are summarized in Tab. 23 and Tab. 24. It should be noted that the computation leads to different elastic properties of the earlywood and latewood cell wall. This contradicts the results from Section 5.5, where the S_2 layer only was considered in the homogenization thus suggesting the same cell wall stiffness of both the earlywood and latewood. Although the microfibril angle is higher, the resulting values at the level of cell wall are also higher than that mentioned in Tab. 19, which is caused by different assumptions and input values. The influence of the wood porosity is covered by the next step. The Mori-Tanaka is employed in the same way as in Section 6.3 and the effective coefficients of hygroexpansion are computed according to Eq. (7.2). The same assumptions regarding the shape and volume fractions of lumens as for the numerical homogenization were adopted, in the sake of comparison. The numerical homogenization was employed using equations derived in Section 7.2.2. The computation starts at the level of cell wall considering layered structure according to the periodic unit cell (Fig. 27), where the properties of individual layers correspond to those computed by analytical homogenization in Section 7.2.1. The final effective properties at the level of lumens of both approaches are very similar, see Tab. 25.

It is apparent from the presented work, that the knowledge of the properties and volume fractions of individual phases is crucial for the use of homogenization methods. However, the wood is very complex material showing a great variability in all its

characteristics, so all parameters have to be evaluated on average. Modern measurement methods allow us to determine the properties of individual constituents up to the nanometre scale. Advanced microscopes provide a view of the structure of material at high zoom. The development of the homogenization model has to be supported by measurements on various scales. Some of the model improvements based on the findings determined within this thesis will be presented in the following text.

Following the homogenization procedure, the first main task is the determination of the properties and volume fractions of the cell wall constituents, which differ for individual layers. However, it is a demanding process among others due to the complicated extraction of individual phases. Also, the assumed shape of the phases is very important issue. The higher value of MFA estimated from the computation according to [13] shows that the model of microfibril, defined as cellulose surrounded by hemicellulose and lignin represents the reality more precisely than that assumed in Chapters 3 and 6. Furthermore, the deviation angle of microfibrils varies in each layer and its measurement is also very complicated. The estimation of the MFA using the nanoindentation measurement could be satisfactory, whereas the data evaluation is still quite questionable. The solution of the contact with viscoelastic material could be a better choice. Also, the assumption of the layered structure of the cell wall is closer to the actual state. Although, no significant difference was found between the used shapes of inclusions representing pores (Section 6.4) due to the considerable length of the cells, the use of ellipsoids is more accurate. Unfortunately, the lumens cause only the reduction of the effective mechanical properties computed by the Mori-Tanaka method, while the effect of the geometric strengthening of the wood structure is not taken into account. This could be implemented into the computation only by modelling the structure and a subsequent calculation using the finite element method. The representation of growth rings adopted here is also not quite accurate. The gradual change of the porosity between the earlywood and latewood should be taken into account, i.e. the transition zone should be taken into account. The solid wood includes many elements that were not considered, whether natural components, such as rays and resin canals, or defects, e.g. knots. It follows from the above that the wood modelling is a very complex matter and there is still a long way to achieve the ‘correct’ model for the prediction of wood properties.

Nomenclature

General notation

$\boldsymbol{a}$	Vector quantity
$\mathbf{A}$	Matrix quantity
a	Scalar quantity
$\mathbf{I}$	Identity matrix
$\mathbf{A}^{-1}$	Inverse of $\mathbf{A}$
$\mathbf{A}^{T}$	Transpose of $\mathbf{A}$
$\boldsymbol{x}$	Position vector
∇	Gradient operator

Basic quantities

u [-]	Moisture content
ρ_{dry} [kg/m^3]	Oven-dry density
f [-]	Volume fraction
E [GPa]	Modulus of elasticity
ν [-]	Poisson's ratio
G [GPa]	Shear modulus
D [m^2/s]	Moisture diffusion coefficient
λ [$W/m.K$]	Coefficient of thermal conductivity
α_h [-]	Coefficient of hygroexpansion

Homogenization

$\mathbf{M}$	Compliance matrix of the material
$\mathbf{L}$	Stiffness matrix of the material
$\mathbf{A}$	Strain concentration factor
$\mathbf{B}$	Stress concentration factor

Abbreviations

MFA	Microfibril angle
MC	Moisture content
EMC	Equilibrium moisture content
FSP	Fibre saturation point
MOE	Modulus of elasticity
RVE	Representative volume element
RH	Relative humidity in surroundings
PUC	Periodic unit cell

Subscripts and superscripts

lum	Lumens
ew	Earlywood
lw	Latewood
cw	Cell wall
R	Radial
T	Tangential
L	Longitudinal
SC	Self-consistent method
MT	Mori-Tanaka method

List of figures

List of tables

References

1. **Ministerstvo zemědělství.** *Zpráva o stavu lesa a lesního hospodářství České republiky v roce 2015 (Report on the state of forests and forestry in the Czech Republic in 2015).* Praha : Ministerstvo zemědělství, 2016. ISBN 978-80-7434-324-7.

2. **Holmberg, Hans and Sandberg, Dick.** *Structure and Properties of Scandinavian Timber.* Stockholm : HoS Grenarna HB, 1997.

3. **Forest Products Laboratory (U.S.).** *Wood handbook: Wood as an engineering material.* Madison, Wisconsin : s.n., 2010.

4. **Desch, H. E. and Dinwoodie, J. M.** *Timber: structure, properties, conversion and use.* Hampshire : Macmillan Press, 1996. ISBN 0333609050.

5. **Kettunen, Pentti O.** *Wood: Structure and Properties.* Uetikon-Zuerich : Trans Tech Publications Ltd, 2006. ISBN 0878494871;9780878494873.

6. **Tsoumis, George.** *Science and technology of wood: Structure, properties, utilization.* New York : Chapman & Hall, 1991. ISBN 0-412-07851-1.

7. **Fujita, Minoru and Harada, Hiroshi.** Ultrastructure and Formation of Wood Cell Wall. [book auth.] David N.-S. Hon and Nobuo Shiraishi. *Wood and Cellulosic Chemistry.* New York : Marcel Dekker, Inc., 2001.

8. **Smith, Ian, Landis, Eric and Gong, Meng.** *Fracture and fatigue in wood.* Chichester : Wiley, 2003. ISBN 0-471-48708-2.

9. **Hofstetter, Karin, Hellmich, Christian and Eberhardsteiner, Josef.** Development and experimental validation of a continuum micromechanics model for the elasticity of wood. *European Journal of Mechanics - A/Solids.* 2005, Vol. 24, 6, pp. 1030-1053.

10. **Eitelberger, J. and Hofstetter, K.** Prediction of transport properties of wood below the fiber saturation point – A multiscale homogenization approach and its experimental validation: Part I: Thermal conductivity. *Composites Science and Technology.* 2011, Vol. 71, 2, pp. 134-144.

11. **Mayo, S. C., Chen, F. and Evans, R.** Micron-scale 3D imaging of wood and plant microstructure using high-resolution X-ray phase-contrast microtomography. *Journal of Structural Biology.* 2010, Vol. 171, 2, pp. 182-188.

12. **Šejnoha, Michal, et al.** Effective material properties of wood based on homogenization. *International Journal of Computational Methods and Experimental Measurements.* 2017 (In Press).

13. **Persson, Kent.** *Micromechanical modelling of wood and fibre properties.* Lund University. Lund : KFS i Lund AB, 2000. Doctoral thesis. ISBN 91-7874-094-0.

14. **Eitelberger, Johannes, Svensson, Staffan and Hofstetter, Karin.** Theory of transport processes in wood below the fiber saturation point. Physical background on the microscale and its macroscopic description. *Holzforschung.* 2011, Vol. 65, 3, pp. 337-342.

15. **Eitelberger, J. and Hofstetter, K.** Prediction of transport properties of wood below the fiber saturation point – A multiscale homogenization approach and its experimental validation. Part II: Steady state moisture diffusion coefficient. *Composites Science and Technology.* 2011, Vol. 71, 2, pp. 145-151.

16. **Eitelberger, Johannes and Svensson, Staffan.** The Sorption Behavior of Wood Studied by Means of an Improved Cup Method. *Transport in Porous Media.* 2012, Vol. 92, 2, pp. 321-335.

17. **Zhao, Dongliang, et al.** Measurement Techniques for Thermal Conductivity and Interfacial Thermal Conductance of Bulk and Thin Film Materials. *Journal of Electronic Packaging.* 2016, Vol. 138, 4.

18. **Kollmann, Franz F.P. and Côté, Wilfred A.** *Principles of Wood Science and Technology.* Berlin : Springer, 1968. Vol. I Solid Wood.

19. **Böhm, Helmut J.** *A short introduction to basic aspects of continuum micromechanics.* Vienna : TU Wien, 1998, 2017.

20. **Milton, Graeme W.** *The theory of composites.* Cambridge : Cambridge Univeristy Press, 2004. ISBN 0-511-04092-X.

21. **Dvorak, George J.** *Micromechanics of composite materials.* Dordrecht : Springer, 2013. ISBN 978-94-007-4101-0.

22. **Šejnoha, Michal and Zeman, Jan.** *Micromechanics in practice.* Southampton : WIT Press, 2013. ISBN 978-1-84564-682-0 .

23. **Eshelby, J. D.** The determination of the elastic field of an ellipsoidal inclusion and related problems. *Proceedings of the Royal Society of London. Series A, Mathematical and Physical Sciences.* 1957, Vol. 241, pp. 376-396.

24. **Hashin, Z. and Shtrikman, S.** A variational approach to the theory of the elastic behaviour of multiphase materials. *Journal of the Mechanics and Physics of Solids,*. 1963, Vol. 11, 2, pp. 127-140.

25. **Mori, T. and Tanaka, K.** Average stress in matrix and average elastic energy of materials with misfitting inclusions. *Acta Metallurgica.* 1973, Vol. 21, 5, pp. 571-574.

26. **Hill, R.** Elastic properties of reinforced solids: Some theoretical principles. *Journal of the Mechanics and Physics of Solids.* 1963, Vol. 11, 5, pp. 357-372.

27. **Aboudi, Jacob, Arnold, Steven M. and Bednarcyk, Brett A.** *Micromechanics of composite materials: A generalized multiscale analysis approach.* Oxford : Butterworth-Heinemann, 2013. ISBN: 978-0-12-397035-0.

28. **Parnell, William J.** The Eshelby, Hill, Moment and Concentration Tensors for Ellipsoidal Inhomogeneities in the Newtonian Potential Problem and Linear Elastostatics. *Journal of Elasticity.* 2016, Vol. 125, 2, pp. 231–294 .

29. **Oliver, W. C. and Pharr, G. M.** Measurement of hardness and elastic modulus by instrumental indentation: Advances in understanding and refinements to methodology. *Journal of Materials Research.* Jan. 2004, Vol. 19, No. 1.

30. **Hysitron.** Hysitron service document - Probe Calibration. [Online] [Cited: 30th April 2017.] https://www.hysitron.com/resources-support/education-training/nanoindentation.

31. **Oyen, Michelle L. and Cook, Robert F.** A practical guide for analysis of nanoindentation data. *Journal of the mechanical behavior of biomedical materials.* 2009, Vol. 2, 3, pp. 396-407.

32. **Pavlík, Zbyšek, et al.** Modified lime-cement plasters with enhanced thermal and hygric storage capacity for moderation of interior climate. *Energy and Buildings.* 2016, Vol. 126, pp. 113-127.

33. **Wadsö, Lars.** *Studies of water vapor transport and sorption in wood.* s.l. : Division of Building Materials, LTH, Lund University, 1993. Doctoral thesis.

34. **Eriksson, John, Johansson, Håkan and Danvind, Jonas.** Numerical determination of diffusion coefficients in wood using data from CT-scanning. *Wood and Fiber Science.* 2006, Vol. 38, 2, pp. 334-344.

35. **Fotsing, Joseph Albert Mukam and Tchagang, Claude Wanko.** Experimental determination of the diffusion coefficients of wood in isothermal conditions. *Heat and Mass Transfer.* 2005, Vol. 41, 11, pp. 977-980.

36. **Tong, Liu.** *Moisture transport in wood and wood-based panels: A pre-study of sorption methods.* TräteknikCentrum. Stockholm : s.n., 1987. Rapport P 8712078.

37. **Jansson, Robert.** *Measurement of thermal properties at elevated temperatures – Brandforsk project 328-031.* SP Swedish National Testing and Research Institute. Borås : s.n., 2004. SP Report 2004:46. ISBN 91-85 303-22-4.

38. **Adl-Zarrabi, Bijan, Boström, Lars and Wickström, Ulf.** Using the TPS method for determining the thermal properties of concrete and wood at elevated temperature. *Fire and materials.* 2006, Vol. 30, 5, pp. 359-369.

39. **Vlassak, J. J., et al.** The indentation modulus of elastically anisotropic materials for indenters of arbitrary shape. *Journal of the Mechanics and Physics of Solids.* 2003, Vol. 51, 9, pp. 1701-1721.

40. **Barnett, John R. and Bonham, Victoria A.** Cellulose microfibril angle in the cell wall of wood fibres. *Biological reviews.* 2004, Vol. 79, 2, pp. 461-472.

41. **Gierlinger, Notburga, et al.** Cellulose microfibril orientation of Picea abies and its variability at the micron-level determined by Raman imaging. *Journal of Experimental Botany.* 2010, Vol. 61, 2, pp. 587-595.

42. **Donaldson, Lloyd.** Microfibril Angle: Measurement, Variation and Relationships – A Review. *IAWA Journal.* 2008, Vol. 29, 4, pp. 345-386.